Biomedicine & Pharmacotherapy 170 (2024) 115979

Contents lists available at ScienceDirect

Biomedicine & Pharmacotherapy

journal homepage: www.elsevier.com/locate/biopha

3,3',5,5'-Tetramethoxybiphenyl-4,4'diol triggers oxidative stress, metabolic changes, and apoptosis-like process by reducing the PI3K/AKT/NF-κB pathway in the NCI-H460 lung cancer cell line

Virginia Marcia Concato-Lopes [a,*], Taylon Felipe Silva [a], Mariana Barbosa Detoni [a], Ellen Mayara Souza Cruz [a], Manoela Daiele Gonçalves [b], Bruna Taciane da Silva Bortoleti [a,c], Fernanda Tomiotto-Pellissier [a,c,d], Amanda Cristina Machado Carloto [a], Maria Beatriz Madureira [a], Ana Carolina Jacob Rodrigues [a,c], Jéseka Gabriela Schirmann [e], Aneli M. Barbosa-Dekker [e], Robert F.H. Dekker [f], Ivete Conchon-Costa [a], Carolina Panis [g], Danielle Lazarin-Bidóia [a], Milena Menegazzo Miranda-Sapla [a], Mário Sérgio Mantovani [h], Wander R. Pavanelli [a]

[a] Laboratory of Immunoparasitology of Neglected Diseases and Cancer, Department of Immunology, Parasitology and General Pathology, Center of Biological Sciences, State University of Londrina, PR, Brazil
[b] Laboratory of Biotransformation and Phytochemical, Department of Chemistry, Center of Exact Sciences, State University of Londrina, PR, Brazil
[c] Graduate Program in Biosciences and Biotechnology, Carlos Chagas Institute (ICC), Fiocruz, Curitiba, PR, Brazil
[d] Department of Medical Pathology, Federal University of Paraná, Curitiba, PR, Brazil
[e] Laboratory Research of Bioactive Molecules, Department of Chemistry, Center of Exact Sciences, State University of Londrina, PR, Brazil
[f] Federal Technological University of Paraná, Graduate Program in Environmental Engineering, Campus Londrina, Londrina, PR, Brazil
[g] Laboratory of Tumor Biology, State University of West Paraná, Unioeste, Francisco Beltrao, Brazil
[h] Laboratory of Toxicological Genetics, Department of General Biology, Center of Biological Sciences, State University of Londrina, PR, Brazil

ARTICLE INFO

Keywords:
Treatment
Cancer
Cell Death
Redox Disruption

ABSTRACT

Lung cancer is one of the leading causes of cancer-related deaths in men and women worldwide. Current treatments have limited efficacy, cause significant side effects, and cells can develop drug resistance. New therapeutic strategies are needed to discover alternative anticancer agents with high efficacy and low-toxicity. TMBP, a biphenyl obtained by laccase-biotransformation of 2,6-dimethoxyphenol, possesses antitumor activity against A549 adenocarcinoma cells. Without causing damage to sheep erythrocytes and mouse peritoneal macrophages of BALB/c mice. In addition to being classified as a good oral drug according to *in-silico* studies. This study evaluated the in-vitro cytotoxic effect of TMBP on lung-cancer cell-line NCI-H460 and reports mechanisms on immunomodulation and cell death. TMBP treatment (12.5–200 μM) inhibited cell proliferation at

Abbreviations: LC, Lung Cancer; NSCLC, Non-small cell lung cancer; SCLC, Small cell lung cancer; TMBP, 3,3',5,5'-Tetramethoxybiphenyl-4,4'-Diol; 2,6-DMP, 2,6-Dimethoxyphenol; ROS, Reactive Oxygen Species; DMSO, Dimethyl sulfoxide; SEM, Scanning Electron Microscopy; TEM, Transmission Electron Microscopy; H_2DCFDA, 2',7'-dichlorofluorescein diacetate; MTT, 3-(4,5-dimethylthiazol-2-yl)− 2,5-diphenyltetrazolium bromide; PBS, Phosphate-buffered saline; SBF, fetal bovine serum; Glc, Glucose; TMRE, tetramethyl rhodamine-ethyl-ester; H_2O_2, Hydrogen peroxide; CCCP, Carbonylcyanide *m*-chlorophenylhydrazone; NAC, N-Acetylcysteine; NO, Nitric Oxide; L-NAME, NG-nitro-L-arginine methyl ester; $O_2\bullet^-$, Superoxide anion radical; SOD, Superoxide dismutase; GSH, Reduced Glutathione; LDH, Lactate dehydrogenase; Δψm, Mitochondrial membrane potential; LD, Lipid droplets; NR, Nile red; MDC, monodansylcadaverine; CPT, Camptothecin; ELISA, Enzyme-linked immunosorbent assay; iNOS, Induzivel nitric oxide sintase; ARG-1, Arginase-1; PI3K, phosphatidylinositol-3-kinase; AKT, Protein kinase B; pAKT, Phospho Protein kinase B; NF-κB, Nuclear factor *kappa* B; pNF-κB, Phospho nuclear factor *kappa* B; Nrf2, Erythroid-derived nuclear factor 2; KOH, Potassium hydroxide; Z-DEVD-AMC substrate, Fluorogenic substrate for caspase 3 e 7; Ac-DEVD-CHO inhibitor, Caspase-3 e 7 Inhibitor I, N-Ac-Asp-Glu-Val-Asp-CHO; RIPA, Radioimmunoprecipitation Assay; EDTA, Ethylenediaminetetraacetic acid; TME, tumor microenvironment; STAT-3, signal transducer and activator of transcription 3; EMT, epithelial-mesenchymal transition; $OH\bullet^-$, Hydroxyl radical; OXPHOS, Oxidative phosphorylation; CAT, catalase; PRDXs, Peroxiredoxins; GPXs, Glutathione peroxidases; $ONOO^-$, Peroxynitrite anion; RNS, Reactive Nitrogen Species.

* Correspondence to: Department of Immunology, Parasitology and General Pathology, Laboratory of Immunopathology of Neglected Diseases and Cancer, State University of Londrina – UEL, Rodovia Celso Garcia Cid Campus, CEP: 86057–970, Post Box 10.011 Londrina, PR, Brazil.
E-mail address: vir_93_@hotmail.com (V.M. Concato-Lopes).

https://doi.org/10.1016/j.biopha.2023.115979
Received 1 August 2023; Received in revised form 14 November 2023; Accepted 30 November 2023
Available online 6 December 2023

24, 48, and 72 h. After 24-h treatment, TMBP at IC_{50} (154 μM) induced various morphological and ultrastructural changes in NCI-H460, reduced migration and immunofluorescence staining of N-cadherin and β-catenin, induced increased reactive oxygen species and nitric oxide with reduced superoxide radical-anion, increased superoxide dismutase activity and reduced glutathione reductase. Treatment also caused metabolic stress, reduced glucose-uptake, intracellular lactate dehydrogenase and lactate levels, mitochondrial depolarization, increased lipid droplets, and autophagic vacuoles. TMBP induced cell-cycle arrest in the G2/M phase, death by apoptosis, increased caspase-3/7, and reduced STAT-3 immunofluorescence staining. The anticancer effect was accompanied by decreasing PI3K, AKT, ARG-1, and NF-κB levels, and increasing iNOS. These results suggest its potential as a candidate for use in future lung anticancer drug design studies.

1. Background

Lung cancer (LC), a heterogeneous disease, remains one of the leading causes of cancer-related mortalities worldwide, with an estimated 2.9 million cases by 2040 [1]. In addition, most patients have metastatic disease at the time of diagnosis [1]. Non-small cell lung cancer (NSCLC) accounts for more than 85% of all LCs and is common in both men and women [2]. Available chemotherapy for NSCLC has advanced significantly over the past decade, and platinum-based doublet therapy (e.g., cisplatin in combination with carboplatin) has been successfully implemented [3]. Several side effects, however, remain, including severe kidney problems, allergic reactions, decreased immunity to infection, gastrointestinal upset, bleeding, hearing loss, and also drug resistance, especially if the tumor recurs [4]. Because of the challenges in treating this disease, new therapeutic strategies are needed and should be developed.

Phenolic compounds are naturally present in plants and can be synthesized through various methods, including biocatalysis, which involves the use of enzymes for the transformation of molecular structures [5,6]. One of the advantages of synthesizing compounds through biocatalysis is that it can be part of a green process, as it employs less toxic methodologies. This has been highlighted in research conducted by [7–9]. 3,3',5,5'-Tetramethoxybiphenyl-4,4'-diol (TMBP), a biphenyl (Figure suppl. 1), was obtained by oxidation of 2,6-dimethoxyphenol (2,6-DMP) using laccase produced by the ascomyceteous fungus *Botryosphaeria rhodina* (MAMB-05) [7,8]. Biphenolic compounds have interesting chemical structures and many of these compounds play diverse biological roles [5,6], including fungicidal [10,11], bactericidal [12,13], anti-inflammatory [14,15], antioxidant [16], cell anti-proliferation [17,18], and anti-tumor activity. In a recent study using TMBP on the A549 (lung adenocarcinoma) tumor cell line, our group showed that treatment with TMBP reduced viability, increased reactive oxygen species (ROS) production, induced mitochondrial depolarization, was involved in cell cycle arrest in the G2/M phase, and death by direct apoptosis, without causing toxicity in BALB/c mouse peritoneal macrophages and sheep erythrocytes [19].

In this study, using different endpoints, TMBP was shown to reduce cell viability and migratory potential, promote morphological and ultrastructural changes, followed by apoptosis and autophagy. These phenomena were mediated by an oxidative burst and metabolic damage through decreased levels of PI3K/pAKT/ARG-1/pNF-κB and an increase of the iNOS pathway in NCI-H460 lung cancer cells.

2. Material and methods

2.1. TMBP

The biphenyl 3,3',5,5'-tetramethoxybiphenyl-4,4'-diol (TMBP; $C_{16}H_{18}O_6$, MW 306) was synthesized from 2,6-DMP using laccase from *Botryosphaeria rhodina* MAMB-05 under conditions previously described [20]. The resulting yellow solid was identified by ^{1}H NMR (CDCl3, 400 MHz) at δ 3.98 (s, 12 H), 6.73 (s, 4 H), 5.56 (s, 2 H), purity 99%, and melting point 185–188 °C. A stock solution of TMBP was prepared in 1% dimethyl sulfoxide (DMSO) (Sigma-Aldrich, St. Louis, MO, USA); the concentration of DMSO was kept at a maximum of 0.06% in all experiments.

2.2. Cell culture

The established NSCLC line, NCI-H460 (large cell carcinoma), from Frederick Ma (National Cancer Institute, Bethesda, MD, USA) was kindly provided by the Toxicological Genetics Laboratory-UEL. The cell was cultured in Roswell Park Memorial Institute (RPMI) 1640 culture medium (Life Technologies, Carlsbad, CA, USA) supplemented with 10% fetal bovine serum (FBS) (GIBCO, Invitrogen, New York, USA), 100 U/mL penicillin and 100 μg/mL streptomycin (Santa Cruz Biotechnologies, Dallas, TX, USA), and incubated at 37 °C under 5% CO_2.

2.3. Cell viability assay

NCI-H460 cells (10^4 cells/well) were treated with TMBP (range 12.5–100 μM) or cisplatin (CIS) (50 μM), and cytotoxicity was assessed at 24, 48, and 72 h. MTT assays were performed as previously described [19]. Briefly, the cells were washed, and MTT (0.33 mg/mL) (Sigma-Aldrich) was added to the cells and then incubated for 3 h at 37 °C. The MTT product formed (formazan crystals) was diluted with 100 μL of DMSO and measured spectrophotometrically at 550 nm. The half-maximal inhibitory concentration (IC_{50}) curve was calculated by logarithmic regression using GraphPad Prism 8 software for the above times. The IC_{50} at 24 h was used for the remaining experiments. Micrographs of TMBP-treated IC_{50} cells were taken using an EVOS Microscope FL Auto Cell imaging system (Thermo-Fisher Scientific, Multiskan GO, Waltham, MA, USA) at 100 × magnification.

2.4. Morphological and ultrastructural analysis of NCI-H460 cells by scanning electron microscopy (SEM) and transmission electron microscopy (TEM)

Scanning electron microscopy (SEM) of the NCI-H460 cell line was performed to analyze morphological changes in the cell surface topography [21]. Briefly, cells (10^5 cells/well) were seeded into 24-well plates, incubated (37 °C, 5% CO_2) and treated with IC_{50}-TMBP for 24 h at 37 °C and fixed with 2.5% glutaraldehyde in 0.1 M sodium cacodylate buffer (pH 7.4). The cells were then dehydrated through increasing concentrations of ethanol (30–100%), subjected to critical point drying (Baltec SCD-030, Balzers, Liechtenstein), and metallized with gold for visualization using a high-resolution FEI SCIOS (Oregon, USA) double beam electron microscope (Thermo Fisher Scientific, Massachusetts, United States).

To assess ultrastructural changes in the TMBP-treated cells by TEM (JEOL USA JEM 1400, Tokyo, Japan, transmission electron microscope), cells were treated and fixed similarly as described above. The samples were then postfixed with 1% OsO_4, 0.8% potassium ferrocyanide, and 10.0 mM $CaCl_2$ in 0.1 M sodium cacodylate buffer (pH 7.4) for 1 h at room temperature and protected from light. The samples were then washed in 0.1 M sodium cacodylate buffer and dehydrated in increasing concentrations of acetone (30–100%). The total acetone content was gradually replaced by EPON™ epoxy resin (Electron Microscopy

Sciences, Hatfield, United States) by cell diffusion and polymerized at 60 °C for 72 h. Nanoscale sections (60–70 nm) were sliced with an ultramicrotome (PowerTomer BMC - Germany) and contrasted with 5% uranyl acetate and 2% lead citrate. Finally, the samples were analyzed by TEM. The NCI-H460 cell line maintained in RPMI culture medium without TMBP treatment was used as a negative control.

2.5. Cell scratch assay

NCI-H460 cells (10^6 cells/well) were seeded into 6-well plates and incubated (37 °C, 5% CO_2) to confluence. We then created a 'scratch' in the monolayer by gently passing a 200 μL pipette tip over the bottom of each well. This passage created a discontinuity in the monolayer whose cells at the edge tended to migrate into the empty spaces. The cells were next treated with IC_{50}-TMBP and photomicrographs (40 × objective) were taken at different times (0, 12, and 24 h) using an EVOS FL Auto 2 microscope (Thermo Scientific, USA). Cell migration was assessed as the free area (region without cells) measured using Image-Pro plus program software (ImageJ), while the percentage decrease in the area was characterized by the cell migration index. Assays were performed in triplicate from each group tested.

2.6. Immunofluorescence (IF) staining

NCI-H460 cells (10^5 cells/well) were seeded in 24-well plates containing coverslips and treated with the 24 h IC_{50} value of TMBP at 37 °C. The assay was performed as described by Duplancic and Kero (2021) [22]. Briefly, background blocking was performed using Abcam Protein Block (ab64226; Abcam, UK) for 25 min after the antigen retrieval. The following primary and secondary antibodies used for IF staining (24 h at 4 °C) were from Santa Cruz Biotechnology (USA): N-cadherin (1:1000), β-catenin (1:500), and STAT-3 (1:1500). Secondary antibodies were used at dilution 1:2000: anti-mouse Texas red (RED) and anti-rabbit Alexa Fluor 488 (GREEN). Cell nuclei were stained with diamidino-2-phenylindole (DAPI, Sigma-Aldrich, USA). The slides were mounted with glycerol and kept protected from light under a fluorescence microscope for later observation. The intensity and localization of the immunoreactivity were analyzed with the Motic BA 410E fluorescence microscope and MOTICAM ProS5 Plus (40 × objective lens). The merge of DAPI and Texas Red images was performed using the Image J software (NIH, USA).

2.7. Analysis of reactive oxygen species (ROS)

ROS generation was assessed by the conversion of non-fluorescent H_2DCFDA to highly fluorescent 2',7'-dichlorofluorescein (DCF) by intracellular free radicals. Briefly, ROS scavenger (N-acetylcysteine – NAC, 5.0 M) was added, or not added, to the NCI-H460 cells 2 h before they received treatment with IC_{50} of TMBP, and were incubated for 24 h at 37 °C. After this period, the cells were washed, and H_2DCFDA solution (10.0 M) was added and left in the dark for 45 min. Fluorescence intensity was quantified using a Glomax® spectrophotometer (Promega, USA) (excitation: 488 nm; and emission: 530 nm). Untreated cells were used as a negative control, and H_2O_2 (0.04%) was used as a positive control. Data were normalized and expressed in arbitrary units.

2.8. Determination of nitrite; an estimate of nitric oxide (NO) levels

NO levels were determined based on the Griess method. NCI-H460 cells (10^5 cells/well) were treated, or not, with the non-specific iNOS inhibitor (L-NAME, NG-nitro-L-arginine methyl ester, Sigma-Aldrich, USA) (25uM) for 1 h before treatment with IC_{50} of TMBP and incubated for 24 h. The supernatant of the samples was collected and analyzed according to Cataneo et al., (2019) [23]. Briefly, 60 μL of supernatant was added to 60 μL of Griess reagent (1% sulfanilamide and 0.1% N-(1-Naphthyl) ethylenediamine in 5% orthophosphoric acid (H3PO4)), incubated for 10 min, protected from light, at room temperature, and read on a plate reader (Thermo Scientific, Multiskan GO, USA) at 550 nm. For quantification, serial dilutions of $NaNO_2$ were used. Untreated cells were used as a negative control.

2.9. Resazurin assay

To assess whether cells treated with IC_{50} of TMBP would alter viability in the presence or absence of the inhibitors NAC and L-NAME, the resazurin assay was performed as follows. NCI-H460 cells (10^5 cells/well) were seeded in 24-well plates and incubated (24 h at 37 °C). After this period, NAC (5 M) or L-NAME (50 μM) was added 2 h and 1 h before, respectively, with or without IC_{50}-TMBP treatment and incubated (24 h at 37 °C). Resazurin (60 μM) was then added and left for 2 h, and the fluorescence intensity was quantified in a Glomax® spectrophotometer (520 nm excitation and 580 nm emission). Data were normalized and expressed in arbitrary units.

2.10. Superoxide anion production

The production of superoxide anion radical ($O_2\bullet^-$) was determined by the reduction of the Redox dye nitro blue tetrazolium (1 mg/mL; NBT, Sigma-Aldrich). NCI-H460 cells (10^4 cells/well) were treated with IC_{50}-TMBP, incubated for 24 h, washed with PBS, and subsequently, 100 μL of NBT solution was added and incubated at 37 °C for 1 h. The supernatant was removed, and the formazan precipitate was then solubilized by adding 60 μL of 2.0 M KOH and 60 μL of DMSO. The optical density was measured spectrophotometrically at 600 nm in a microplate reader (Multiskan GO Microplate Spectrophotometer, Thermo Scientific, and Vantaa, Finland). Untreated cells were used as a negative control, and phorbol myristate acetate (PMA) treatment was used as a positive control.

2.11. Superoxide dismutase (SOD) activity

SOD activity was determined based on the enzyme capacity to inhibit auto-oxidation of pyrogallol, as described by Marklund and Marklund [24]. For the determination of SOD activity, NCI-H460 cells (10^5 cells/well) were seeded, treated with the IC_{50} of TMBP, and incubated for 24 h at 37 °C. Subsequently, the cells submitted a cycle of freezing at − 80 °C and thawing at 37 ∘C for 30 min each. Total protein was determined on the cell lysate by the Lowry method [25]. The data were normalized as mg protein/mL. Untreated cells were used as a negative control.

2.12. Reduced glutathione (GSH)

Reduced L-glutathione (GSH) was measured to determine the intensity of oxidative stress. NCI-H460 cells (10^5 cells/well) were seeded and treated with TMBP as described above. After 24 h, GSH quantification was performed according to the method described by Rahman et al., 2007 [26]. Concentrations were determined based on a standard curve constructed with serial dilutions of GSH. Untreated cells were used as a negative control.

2.13. Glucose assay

To assess glucose uptake, NCI-H460 cells (10^5 cells/well) were seeded in 24-well plates, treated with IC_{50} TMBP, and incubated for 24 h at 37 °C. The enzymatic-colorimetric glucose assay was performed according to the manufacturer's kit instructions (Gold Analisa Diagnostics, Minas Gerais, Brazil). Briefly, 1.0 μL aliquots of the supernatant from the treated or standard samples were transferred to a 96-well plate, followed by the addition of 100 μL of the glucose kit reagent, and the mixture incubated for 10 min at 37 °C. The reading was performed in a preheated spectrophotometer (37 ºC) at 505 nm. Untreated cells were used as a

negative control.

2.14. Lactate dehydrogenase (LDH) Activity

To evaluate the LDH activity, NCI-H460 cells (10^6 cells/well) were seeded in 6-well microplates and treated with IC_{50}-TMBP for 24 h at 37 °C. After this period, the cell supernatant was collected to measure extracellular LDH. For the determination of intracellular LDH activity, the cells that had adhered to the multiplate wells were first washed twice with PBS, and water was added to perform 3 repetitions of freezing (−80 °C) and thawing in a heated waterbath, in order to lyze the cells. The intra- and extracellular LDH assays were performed according to the kit instructions (Gold Analisa Diagnóstico, Minas Gerais, Brazil). Untreated cells were used as a negative control.

2.15. Lactate analysis

For intracellular lactate measurement, cells were lyzed (as described above) and the procedures were followed according to the kit datasheet (Katal Biotecnológica, Belo Horizonte, MG, Brazil). Spectrophotometric reads (540 nm) were performed using a microplate reader (Thermo Scientific Multiskan). Untreated cells were used as a negative control.

2.16. Determination of mitochondrial membrane potential ($\Delta\Psi m$)

We performed the analysis of mitochondrial membrane potential through tetramethyl rhodamine-ethyl ester (TMRE; Sigma-Aldrich, USA). NCI-H460 cells (10^4 cells/well) were treated with IC_{50}-TMBP for 24 h at 37 °C. The assay was performed as described by Concato et al. (2020) [19]. Untreated cells were used as a negative control and carbonylcyanide *m*-chlorophenylhydrazone (CCCP) (100 μM) was used as a positive control. Data were normalized and expressed in arbitrary units.

2.17. Detection of lipid droplets (LD)

To determine LD accumulation, NCI-H460 cells (10^4 cells/well) were treated with IC_{50}-TMBP for 24 h at 37 °C and stained with 10 μg/mL Nile red (NR; Sigma-Aldrich, St. Louis, MO, USA) for 30 min. The assay was performed according to Concato et al. [19]. Untreated cells were used as a negative control, and PBS treatment was used as a positive control. Data were normalized and expressed in arbitrary units.

2.18. Determination of the formation of autophagic vacuoles

The formation of autophagic vacuoles was evaluated by staining with monodansylcadaverine (MDC; Sigma-Aldrich, St. Louis, MO, USA), according to Concato et al. [19]. Briefly, NCI-H460 cells (10^4 cells/well) were treated with IC_{50}-TMBP for 24 h at 37 °C and MDC was then added and left for 1 h. The fluorescence intensity was quantified by spectrophotometry (Glomax, Promega, USA) (excitation 380 nm and emission 525 nm). Untreated cells were used as a negative control, and PBS treatment was used as a positive control. Data were normalized and expressed in arbitrary units.

2.19. Cell cycle analysis

NCI-H460 cells (10^6 cells/well) were treated with IC_{50}-TMBP for 24 h at 37 °C. The assay was performed as described by Concato et al. (2020) [19]. Briefly, the cell suspension was subjected to centrifugation at 1500 rpm for 5 min and the cell pellet resuspended in 300 μL of PBS. Subsequently, a solution containing 0.05% ribonuclease A (RNAse A) (Sigma, St. Louis, MO, USA) was added and incubated for 30 min at 37 °C. In the end, a solution of 0.1% sodium citrate and 1% Triton-X100 was added with 50 μg propidium iodide (PI) (Sigma, St. Louis, MO, USA) for 30 min. The fluorescence was estimated using a Muse Cell Analyzer (Merck Millipore), with 5000 events. The DNA content was analyzed, and the percentage of cells in different phases of the cycle (G1, S, and G2/M) were estimated according to the fluorescence intensity.

2.20. Cell death assay

NCI-H460 cells (10^6 cells/well) were treated with IC_{50}-TMBP for 24 h, and phosphatidylserine exposure was detected using Annexin-V FITC (Invitrogen, Eugene, USA), and cellular membrane integrity was detected with PI (0.50 μg/ mL) (Sigma, St. Louis, MO, USA). The assay was performed and described by Concato et al. [19].

2.21. Caspase-3/7 Assay

Caspase-3/7 protease activity was measured using the EnzChek™ Caspase-3/7 Assay Kit (Invitrogen™). Briefly, NCI-H460 cells (10^6 cells/well) were treated with IC_{50}-TMBP for 24 h, washed with PBS, and incubated at − 80 °C for lysis. Lysis buffer (Triton X-100 in 1% PBS) was subsequently added and the solution was left for 30 min. This was followed by the addition of kit reagents (i.e., reaction buffer, dithiothreitol, and 5.0 mM Z-DEVD-AMC substrate) and incubated for 30 min. On completion of the reaction, the increase in fluorescence intensity, which is indicative of cleavage of the Z-DEVD-AMC substrate, was fluorometrically read (GloMax, Promega, USA) at excitation and emission wavelengths of 342 and 441 nm, respectively. The reactions were performed with and without the Ac-DEVD-CHO inhibitor (1 mM). Data were normalized and expressed in arbitrary units.

2.22. Protein Extraction and Enzyme-linked Immunosorbent Assay

NCI-H460 cells (10^6 cells/well) were plated and treated with IC_{50}-TMBP for 24 h, followed by washing with sterile PBS to remove non-adherent cells in the plate wells. The adhered cells were incubated with RIPA lysis buffer (150 mM sodium chloride, 1% triton X-100, 0.5% sodium deoxycholate, 0.1% sodium dodecyl sulfate, 5 mM EDTA, 50 mM Tris, pH 8.0) overnight at − 80 °C. The cell lysate was collected and centrifuged at 13,000 × *g* for 20 min at 4 °C, the supernatant recovered and transferred to a new tube and the total protein concentration was quantified using NanoVue Plus reagent (Biochrom, USA). The protein concentration of all samples was normalized to 20 μg/mL, and a 100-μL aliquot was added in a 96-well ELISA plate for adsorption of proteins overnight at 4 °C. This was followed by adding a blocking buffer (ELISA/ELISPOT, eBioscience™, USA) and the plate was incubated for 1 h. The wells were then washed 3x with wash buffer (PBS in 0.5% Tween-20) and incubated with primary antibodies: anti-human PI3K, AKT, pAKT, arginase-1, NF-κB, pNF-κB, iNOS, and Nrf2 (Santa Cruz Biotech, USA) for 2 h at room temperature. The wells were then washed (wash buffer) to remove unbound antibodies, followed by the addition of universal biotinylated secondary antibody (LSAB2 System-HRP, Dako, USA) and incubated for 1 h. The wells were then washed (wash buffer), followed by the addition of streptavidin-HRP (LSAB2 System-HRP, Dako, USA) and incubated for 1 h. After the incubation time, the wells were washed 5 times (wash buffer) and 100 μL of TMB substrate solution (eBioscience™, USA) was added, followed by incubation for 30 min, and then 100 μL of stop solution (0.5 M sulfuric acid) was added. The plate was read in a microplate reader at 450 nm (GloMax, Promega, USA).

2.23. Statistical analysis

Data are expressed as the mean ± standard error of the mean. Three independent experiments were performed, each with duplicate data sets, and analyzed with GraphPad Prism 8 statistical software (GraphPad Software, Inc., USA, 500.288). Significant differences between groups were determined through t-tests or one-way ANOVA followed by Tukey's test for multiple comparisons. A result was considered statistically significant if $p < 0.05$. Values were also categorized fallows: * ($p < 0.05$); ** ($p \leq 0.01$); *** ($p \leq 0.001$); **** ($p \leq 0.0001$).

3. Results

3.1. TMBP treatment reduces proliferative activity in NCI-H460 cell line

We first evaluated the cell viability after treatment with TMBP (12.5–200 μM) or cisplatin (CIS) (50 μM) for 24–72 h. The vehicle (DMSO) showed no toxic effect at any of the times tested. At 24, 48, and 72 h, the concentrations of TMBP within the range 25–200 μM reduced the proliferation of the NCI-H460 cells ($p \leq 0.0001$), but the effects were more pronounced at 72 h. The concentration of 12.5 μM TMBP also affected cell viability which was reduced by 20% during this period (Fig. 1A). The IC_{50} was calculated for all the times tested (24, 48, and 72 h), resulting in the respective values of 152 μM (± 0.07), 73 μM (± 0.03), and 42 μM (± 0.03) (Table 1). The IC_{50} at 24 h was used for the following experiments, as previously described [19] and representative microscopic images showed morphological changes, such as rounding and apoptosis-like signs (white arrow) (Fig. 1B).

Table 1
The IC_{50} in lung cancer NCI-H460 cell line after TMBP treatment for 24–72 h.

IC_{50} (± SEM)			
Cell Type	24 h	48 h	72 h
NCI-H460	152 μM (± 0.07)	73 μM (± 0.03)	42 μM (± 0.03)

IC_{50} – Half-maximal inhibitory concentration; SEM – standard error of the mean.

3.2. TMBP induces morphological changes in NCI-H460 cell line

SEM was used to determine the morphological changes induced by TMBP treatment in the NCI-H460 cell line. Untreated cells (Fig. 2 A, B) showed normal characteristics such as firm adherence to the substrate, intact cell membrane, presence of lamellipodia, filopodia, microvilli throughout the cell surface, and well-preserved structures. Cells treated with IC_{50}-TMBP, however, showed rounded shapes, reduction of lamellipodia, irregular cell surface, and absence and/or reduction of microvilli. TMBP treatment induced a reduction in cell surface blebbing, indicating the release of large oncosomes; a type of extracellular vesicle characteristic of cells with a more aggressive profile and metastatic

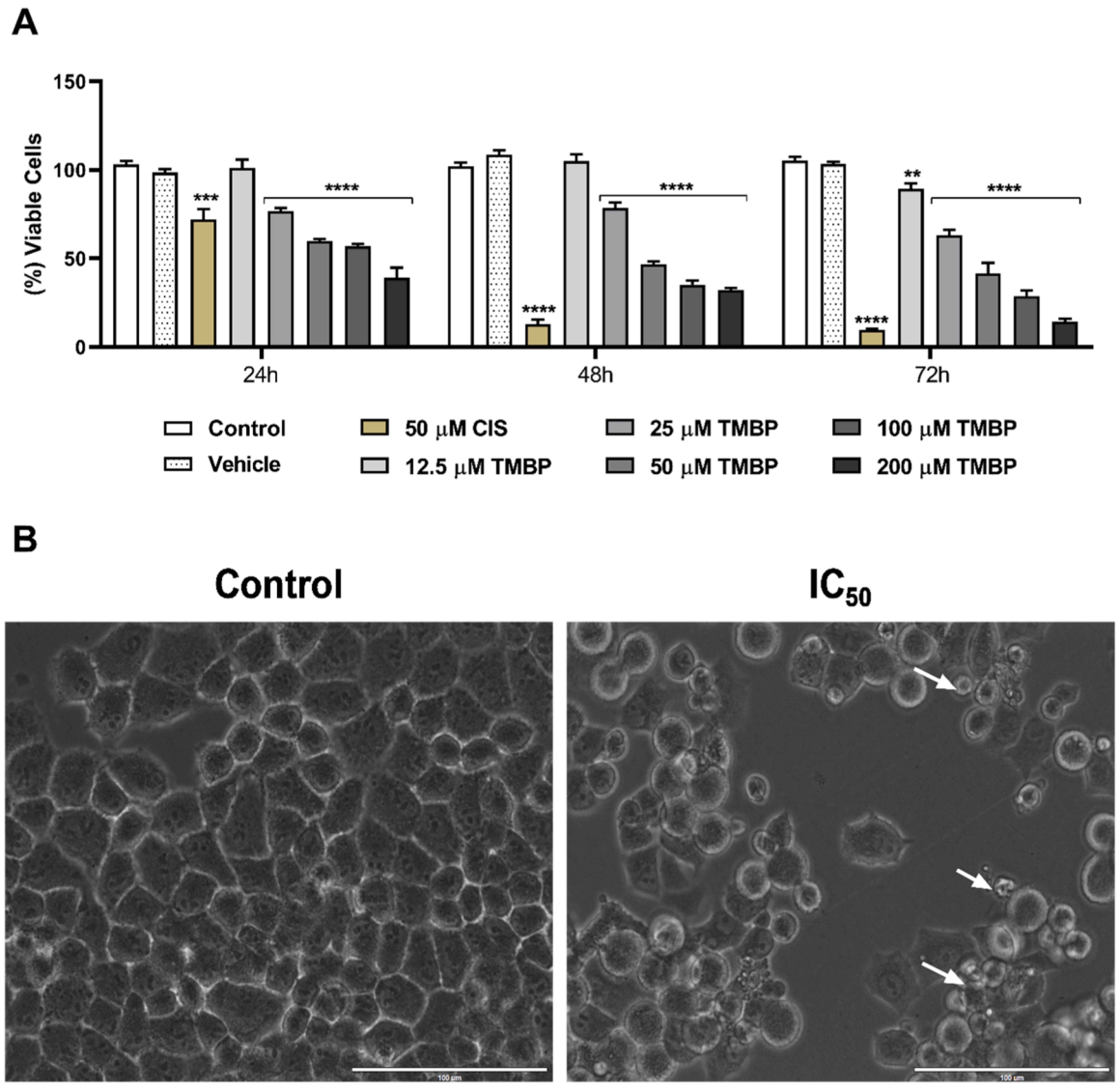

Fig. 1. : TMBP reduced the viability of the human cancer cell line NCI-H460 at different concentrations. NSCLC cells were treated with TMBP for 24, 48, and 72 h. The relative survival rate (A) was determined by the MTT test. After determining the half-maximal inhibitory concentration (IC_{50}) of TMBP, representative images were taken by light microscopy (1000 ×) (**B**). Blebbing around the cells (white arrow). Values are expressed as mean ± SEM. Significant difference with ** $p \leq 0.01$, *** $p \leq 0.001$ and **** $p \leq 0.0001$ vs. control; vehicle (DMSO 0.06%); CIS, cisplatin. Scale bar = 100 μm.

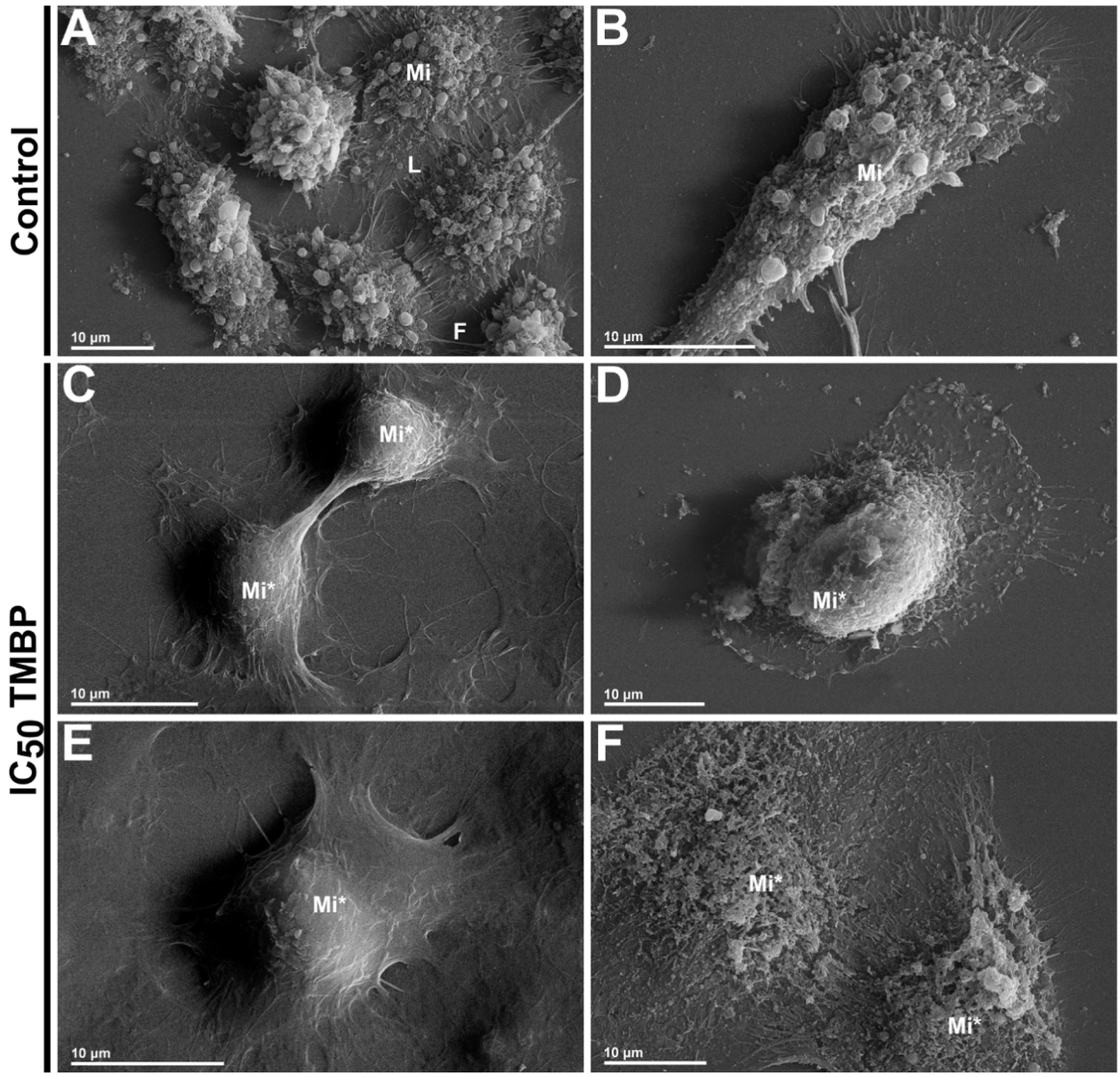

Fig. 2. : Effect of TMBP treatment on the morphology of NCI-H460 cells. Morphological changes were observed by scanning electron microscopy after treatment with TMBP for 24 h. (**A-B**) Control, untreated cells; (**C-F**) cells treated with IC_{50} of TMBP (152 µM). (Mi) microvilli, (Mi*) microvilli alterations, (L) lamellipodia and (F) filopodia. Scale bars = 10 µm (A-F).

potential (Fig. 2 C-F). Our data demonstrated that in addition to reducing proliferation, TMBP treatment was also able to alter the morphology of the cells, contributing to their inability to move and reducing malignancy.

3.3. TMBP treatment reduces migratory capacity and N-cadherin/β-catenin markers in the NCI-H460 cell line

The effect of IC_{50}-TMBP treatment on the migratory potential of NCI-H460 cells was assessed using the *in vitro* wound healing assay (Fig. 3). The filling of the scratched area by migrating cells was monitored at regular time intervals (0, 12, and 24 h) and illustrated by representative images (Fig. 3A). Quantitative analysis concerning the time traveled revealed that in the control group, cells migrated to the wound site, however, those that received TMBP treatment showed an increase in the scratched area in comparison to time 0 h ($p < 0.0001 \pm 0.29$) (Fig. 3 B-C). Corroborating these data, after 24 h of treatment with IC_{50} of TMBP, we observed reduced levels of fluorescence intensity of β-catenin ($p < 0.0001 \pm 1.22$) and N-cadherin ($p < 0.0001 \pm 1.56$) compared to the untreated group (Fig. 3 D-F).

3.4. TMBP induces oxidative stress in the NCI-H460 cell line by a ROS/NO-dependent process

ROS production in TMBP-treated cells was analyzed by fluorescence. Fig. 4B demonstrated that exposure of cells to TMBP resulted in a 2-fold increase in fluorescence intensity compared to the control ($p < 0.0001 \pm 0.09$). The antioxidant N-acetyl cysteine (NAC) was used to confirm the elevation of ROS. The addition of NAC effectively blocked TMBP-induced ROS in NCI-H460 cells and restored viability (Fig. 4 A, B). In the same way, when the levels of NO post-treatment with TMBP were evaluated, an increase of 80% ($p < 0.0001 \pm 0.041$) levels of this mediator was observed. The addition of L-NAME, a nitric oxide synthase (NOS) inhibitor, restored these levels and cell viability (Fig. 4 A, C).

Superoxide anion radical ($O_2\bullet^-$) is one of the most frequently generated ROS in the cell and can react with other molecules to form potent reactive species, such as peroxynitrite, or be dismutated by SOD to produce O_2 and H_2O_2 [27,28]. After treatment of the cells with TMBP, we observed reduced $O_2\bullet^-$ levels (Fig. 4D) and increased SOD activity (Fig. 4E). Furthermore, a reduction of the antioxidant GSH (Fig. 4F) (which is essential for ROS detoxification) was also observed. These results suggest that TMBP reduces NCI-H460 cell viability mediated by

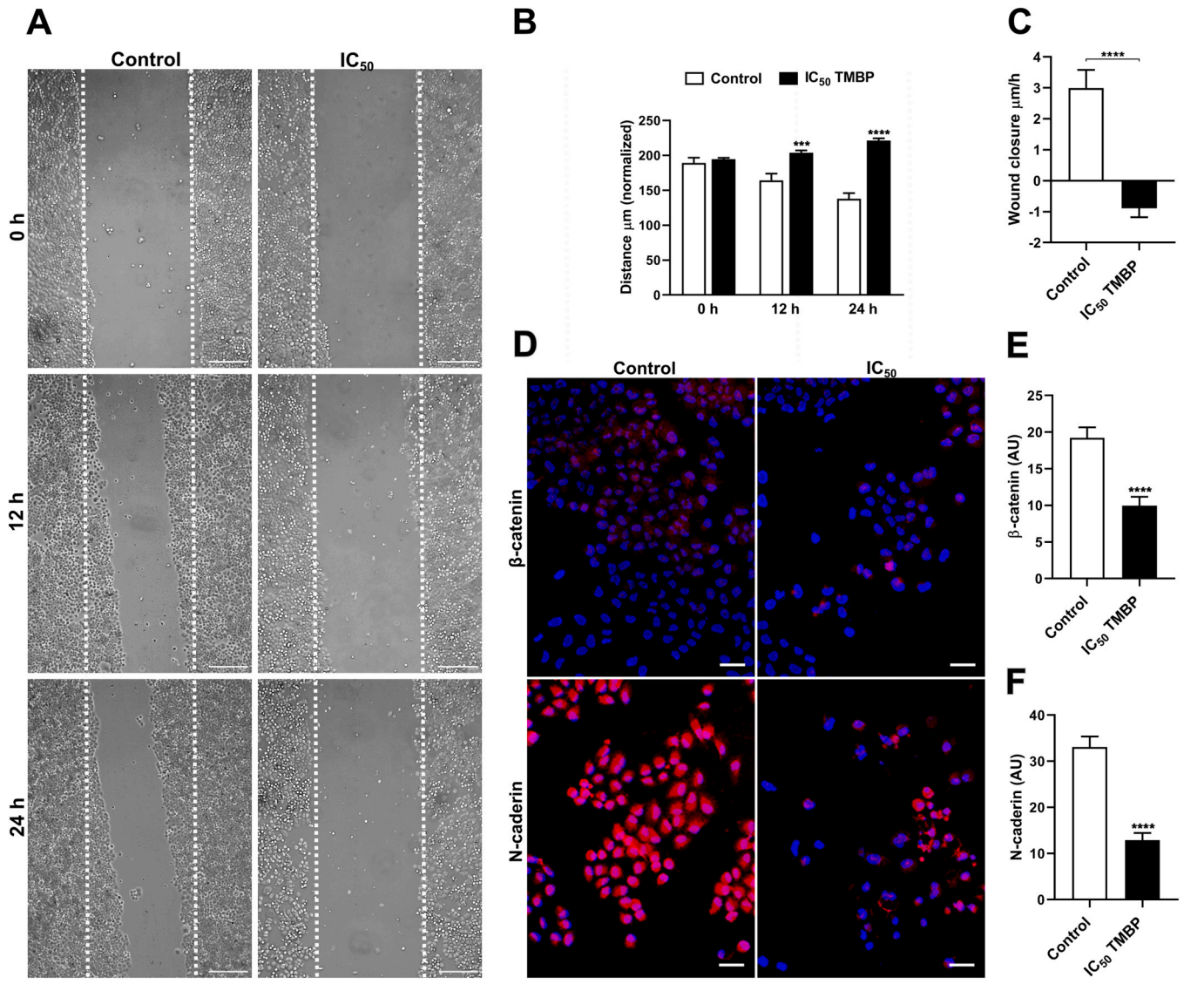

Fig. 3. : TMBP treatment inhibited NCI-H460 cell migration, with cell retraction and reduced N-cadherin and β-catenin staining. A scratch assay was performed to observe the effect of treatment on cell migration over time (0, 12 and 24 h) (**A**). The distance of the free surface of these treated cells (**B**) was quantified. The time taken by the cells to reach the wound site was also quantified (**C**). Immunofluorescence staining of TMBP-treated and control cells to show reduced β-caternin (red) and N-cadherin (red) presence after 24 h (D) (scale bar 2 µm). (E-F) quantification of fluorescence intensity using Image J software. Values represent the mean ± SEM of three different experiments performed in triplicate. Significant difference versus control * ** $p \leq 0.001$ and * ** * $p \leq 0.0001$. Scale bars = 200 µm (A) and 20 µm (D).

increasing levels of ROS/NO molecules.

3.5. TMBP promotes metabolic changes in NCI-460

To assess cellular metabolism, we first examined glucose levels after TMBP treatment of NCI-H460 cells. We observed a reduction in glucose uptake compared to untreated cells ($p \leq 0.0001$) (Fig. 5A). When LDH (which is crucial for converting pyruvate to lactate and vice versa) enzyme activity was assessed, there was a significant 70% increase in extracellular levels and a 65% decrease in intracellular levels ($p > 0.0001$; both activities), indicating cellular damage (Fig. 5 B-C). The levels of lactate (a glucose metabolite of aerobic glycolysis) also decreased compared to the control, with concentrations of 80 mg/dL in the control group and 10 mg/dL in the TMBP-treated groups ($p > 0.0001$) (Fig. 5D).

The mitochondrial membrane was examined in NCI-H460 cells after treatment with IC_{50} of TMBP. A decrease in TMRE fluorescence intensity was observed, indicating a loss of mitochondrial activity ($p \leq 0.01$) (Fig. 5E). Excess intracellular lipids can be stored in LDs to prevent lipotoxicity. During nutrient deprivation, fatty acids are released from LDs for energy production through mitochondrial β-oxidation and the Krebs cycle apoptosis (Cruz et al., 2020). In our results, TBMP treatment induced and increased the level of LD accumulation compared to the control ($p \leq 0.0001$) (Fig. 5F). In addition, we investigated whether treating cells with IC_{50} of TMBP would affect autophagy. We found that the treated group increased the fluorescence intensity, indicating the formation of autophagic vacuoles in NCI-H460 cells ($p \leq 0.0001$) (Fig. 5G).

3.6. TMBP induces structural changes in the NCI-H460 cell line

Ultrastructural evaluation by TEM showed that the control group displayed a homogeneous cytoplasm with regular organelles (mitochondria and endoplasmic reticulum) and without the presence of vacuole-like structures, indicating cellular integrity (Fig. 6 A-B). After TMBP treatment, changes in mitochondrial structures were observed,

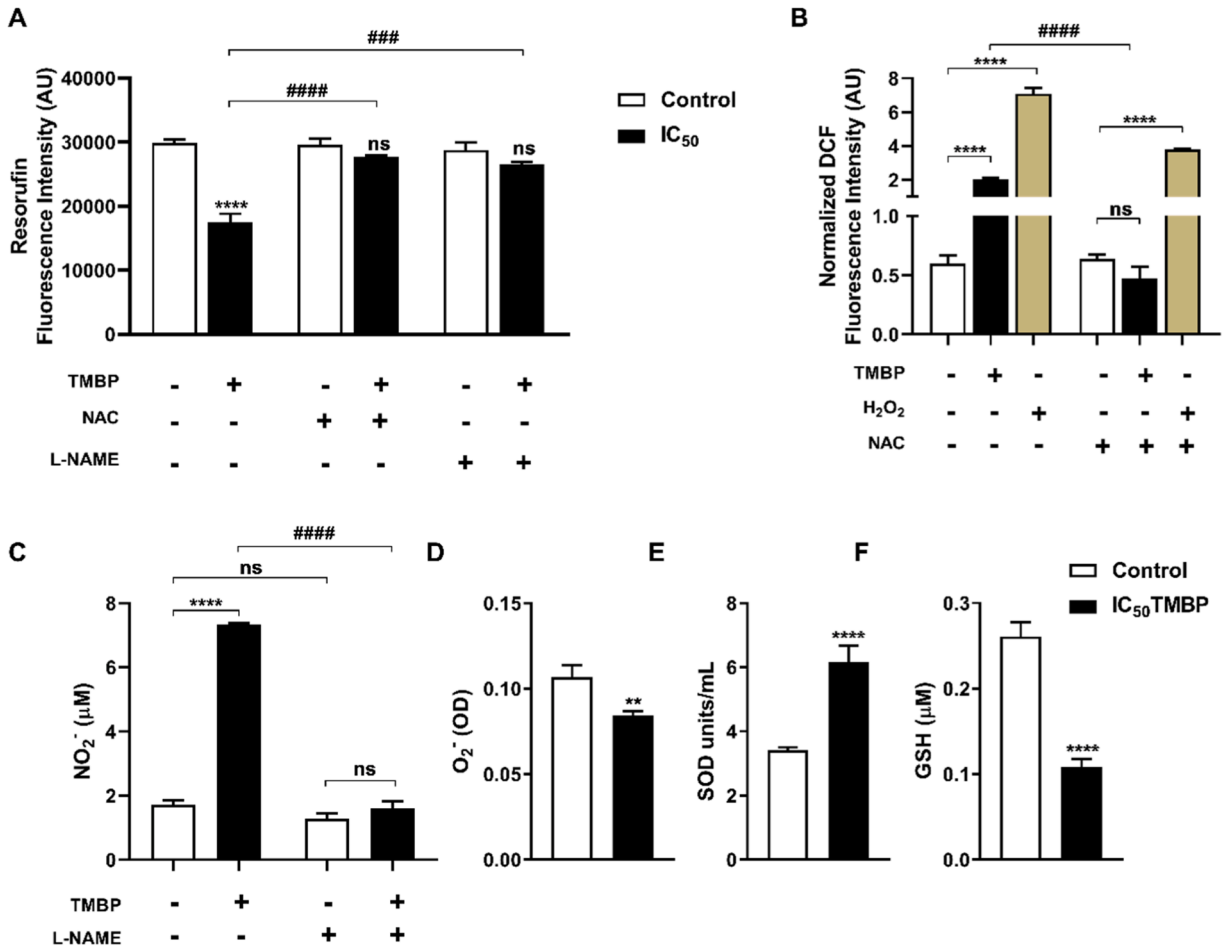

Fig. 4. : TMBP treatment induced oxidative stress in NCI-H460 cells. The viability of cells treated with IC_{50} of TMBP was assessed by resazurin in the presence or absence of NAC or L-NAME (**A**). ROS levels were assessed with H_2DCFDA in the presence or absence of NAC (**B**). Nitric oxide was determined after TMBP treatment in the presence or absence of L-NAME (**C**). Superoxide radical anion was determined using NBT (**D**). SOD and GSH activity were also determined after TMBP treatment (**E-F**). Data are expressed as mean ± SEM of 3 independent experiments performed in triplicate. ns not significant; * * ($p < 0.01$); * ** * ($p \leq 0.0001$) vs. control. $^{###}$ ($p \leq 0.001$) and $^{####}$ ($p \leq 0.0001$) treatment differences.

such as swelling and enlargement of these organelles (m*) (Fig. 6 C-E). These changes were consistent with the data presented above and indicated that mitochondria were damaged. In addition, an intense accumulation of lipid storage droplets (*) and autophagic vacuoles (white arrow) were observed (Fig. 6 C, D, F). Furthermore, the absence of microvilli, filopodia, and lamellopodia (black arrowhead) were also observed (Fig. 6 D-F).

3.7. TMBP promotes cell cycle arrest in the G2/M phase and apoptosis via caspase-3/STAT-3

Analysis of cell cycle distribution also revealed a reduction in the G1 and S phases (51.1% ± 0.86% and 9.5% ± 1.40, respectively) and an accumulation of cells in the G2/M phase (52.7% ± 1.31) (Fig. 7 A-B). Fig. 7 C-D shows that TMBP-treated cells promoted reduced cell viability by 49.75% (± 0.72), increased annexin (24.7% ± 0.85), and co-marking (annexin/PI) (25.15% ± 0.22) compared to the control, indicating cell death by an apoptosis-like process. This was confirmed by the increase in caspase-3/7 activity observed in these cells (Fig. 7E). Also, when evaluated by immunofluorescence the signal transducer and activator of transcription 3 (STAT-3), a reduction of this protein was observed in cells treated with TMBP ($p \leq 0.0001$) (Fig. 7F-G). In contrast, higher staining was observed in the untreated group. These data show that TMBP promoted metabolic damage that disrupted mitosis and progression leading to cell death.

3.8. TMBP acts on the PI3K/AKT/NF-κB pathway and activates iNOS mediated pro-oxidant profile in NCI-H460 tumor cell line

The PI3K/AKT signaling pathway is frequently activated in cancer as it is involved in the regulation of proliferation, survival, inhibition of apoptosis, and cell invasion [34]. These proteins were therefore evaluated by ELISA after treatment with TMBP (Fig. 8). A decrease in PI3K ($p \leq 0.01$) and an increase in total AKT ($p \leq 0.0001$) were observed. The pAKT ($p \leq 0.01$) phosphorylated activated form, however, decreased.

After treatment with TMBP, we observed reduced levels of arginase-1 (ARG-1) ($p < 0.05$) and increased levels of inducible nitric oxide synthase (iNOS) ($p \leq 0.01$). Next, nuclear factor *kappa* B (NF-κB) was evaluated after treatment with TMBP. We observed a decrease in total NF-κB protein levels ($p \leq 0.01$) and its activated phosphorylated form (pNF-κB) ($p \leq 0.04$). Furthermore, when the nuclear factor erythroid 2 related factor 2 (Nrf2) was analyzed, we found that its levels did not significantly differ from the control group ($p > 0.05$).

4. Discussion

Chemoresistance is a common feature and a major cause of treatment failure in NSCLC, leading to tumor recurrence and disease progression. This ability is associated with most available drugs, including cisplatin. The main factors associated with cisplatin resistance are reduced accumulation and inactivation of the drug by binding to various proteins,

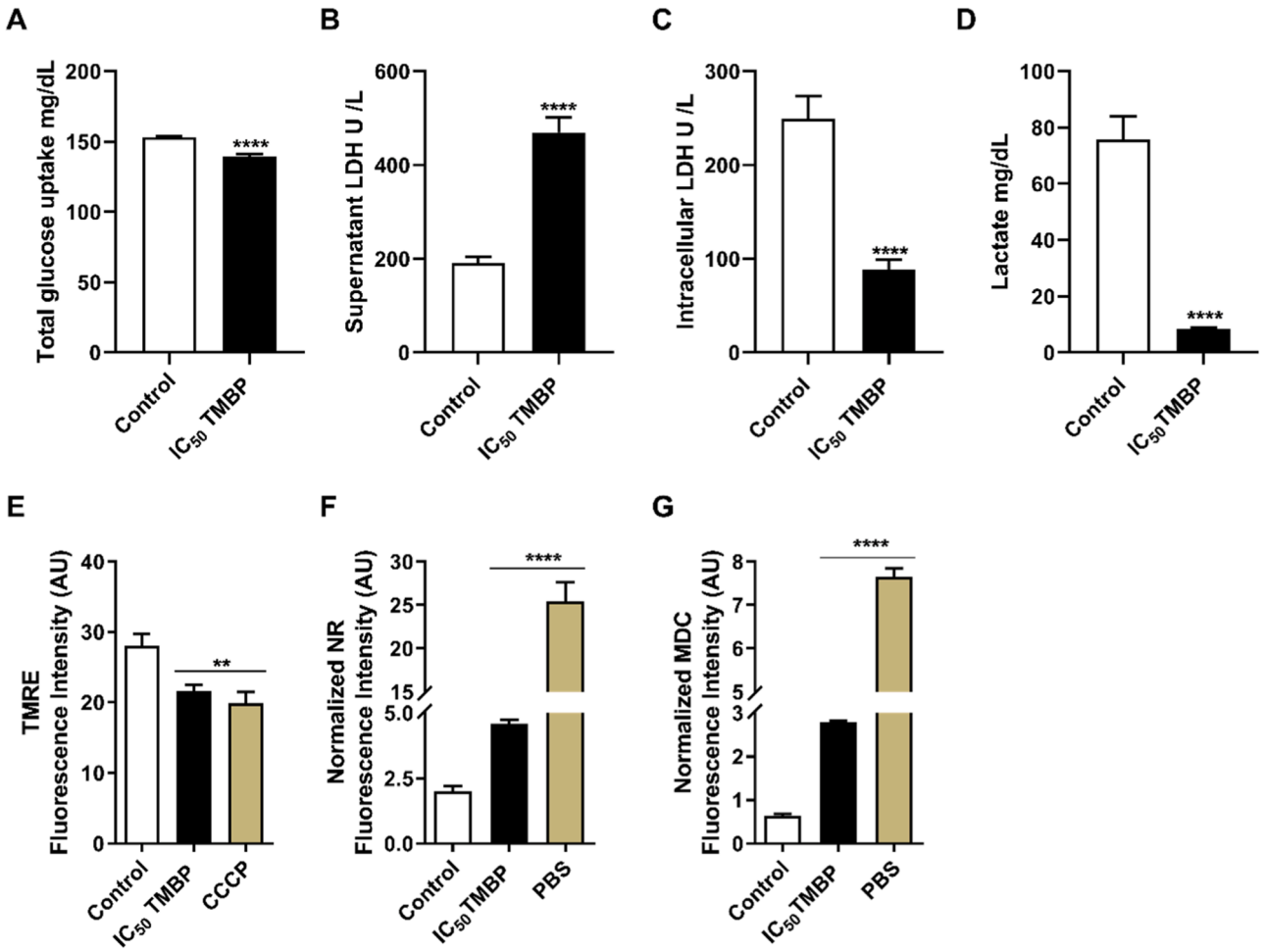

Fig. 5. : TMBP treatment induced metabolic stress in NCI-H460 cells. Cells were treated with TMBP for 24 h. (A) extracellular glucose uptake; (B and C) extracellular and intracellular LDH activity, respectively; and (D) intracellular lactate level. ΔΨm (E), lipid droplets (F), and autophagic vacuoles (G) were quantified by fluorescence. Data are expressed as mean ± SEM of 3 independent experiments, each performed in triplicate. * * ($p < 0.01$); * ** * ($p \leq 0.0001$) vs. control. CCCP, carbonylcyanide *m*-chlorophenylhydrazone; PBS, phosphate-buffered saline.

increased DNA repair, and alteration of various proteins signaling apoptosis [35–37]. In this context, there is a growing interest in microbial biotransformation of drugs and natural products with antitumor activity. This process allows the modification of the relevant chemical molecules, generating new compounds that may be more effective and less toxic. In addition, it is possible to take advantage of the mild conditions under which the reactions take place, with most transformations occurring at temperatures between 20 °C and 40 °C and with aqueous solvents. Although yields are sometimes limited, several options for biological reagents can be manipulated through mutants, aeration, temperature, and culture medium to improve these results [38,39]. Thus, the development of therapeutic strategies that are effective in eliminating aberrant cells and preventing malignant growth is of great interest as it may can expand the possibilities of new approaches for therapeutic applications.

In a previous study, we demonstrated that TMBP exhibited direct cytotoxic effects on the A549 cell line. In addition, *in silico* predictions have shown promising drug-likeness potential for TMBP, indicating high oral bioavailability and intestinal absorption [19]. For the first time, the present study provides new insights into the type of cell death induced by TMBP against the NCI-H460 cell line, demonstrating anti-proliferative activity, metabolic and structural changes (reduced lamellipodia, filopodia, microvilli, and release of large oncosomes). A series of biochemical processes showed that TMBP acts by producing ROS and NO that potentially lead to cell death. Furthermore, TMBP treatment of the cell line reduced protein levels of PI3K/pAKT/ARG-1/pNF-κB and increased iNOS, which may favor increased oxidative stress and promote death in these tumor cells. The significance of our in vitro findings is reinforced by the fact that key components of the TMBP-mediated pathway described have identified cellular self-destruction in lung cancer, and may lead to improved oncotherapy.

Cell proliferation and migration are considered an essential and regulated behavior in several normal physiological processes, such as morphogenesis, embryogenesis, immune cell responses, angiogenesis, tissue repair, cell differentiation, and tissue regeneration [40]. In cancer, cell migration, invasion, and adhesion are phenomena that determine cell plasticity and epithelial-mesenchymal transition (EMT). During the process of EMT, which involves the transformation of cancer cells from a non-motile epithelial phenotype to a migratory mesenchymal-like phenotype, several changes occur in the markers expression. Epithelial markers such as E-cadherin, α-catenin, and β-catenin are down-regulated, while mesenchymal markers like N-cadherin and vimentin are upregulated. This transition closely correlates with increased cell migration and invasion, contributing to cancer progression [41–43].

It is worth noting that in the context of cancer, the stabilization of β-catenin and its subsequent translocation into the nucleus can promote cancer progression, cell proliferation, and metastasis [44–47]. By reducing β-catenin levels, the compound TMBP may actually inhibit the pro-metastatic effects associated with β-catenin. Similarly, the decrease

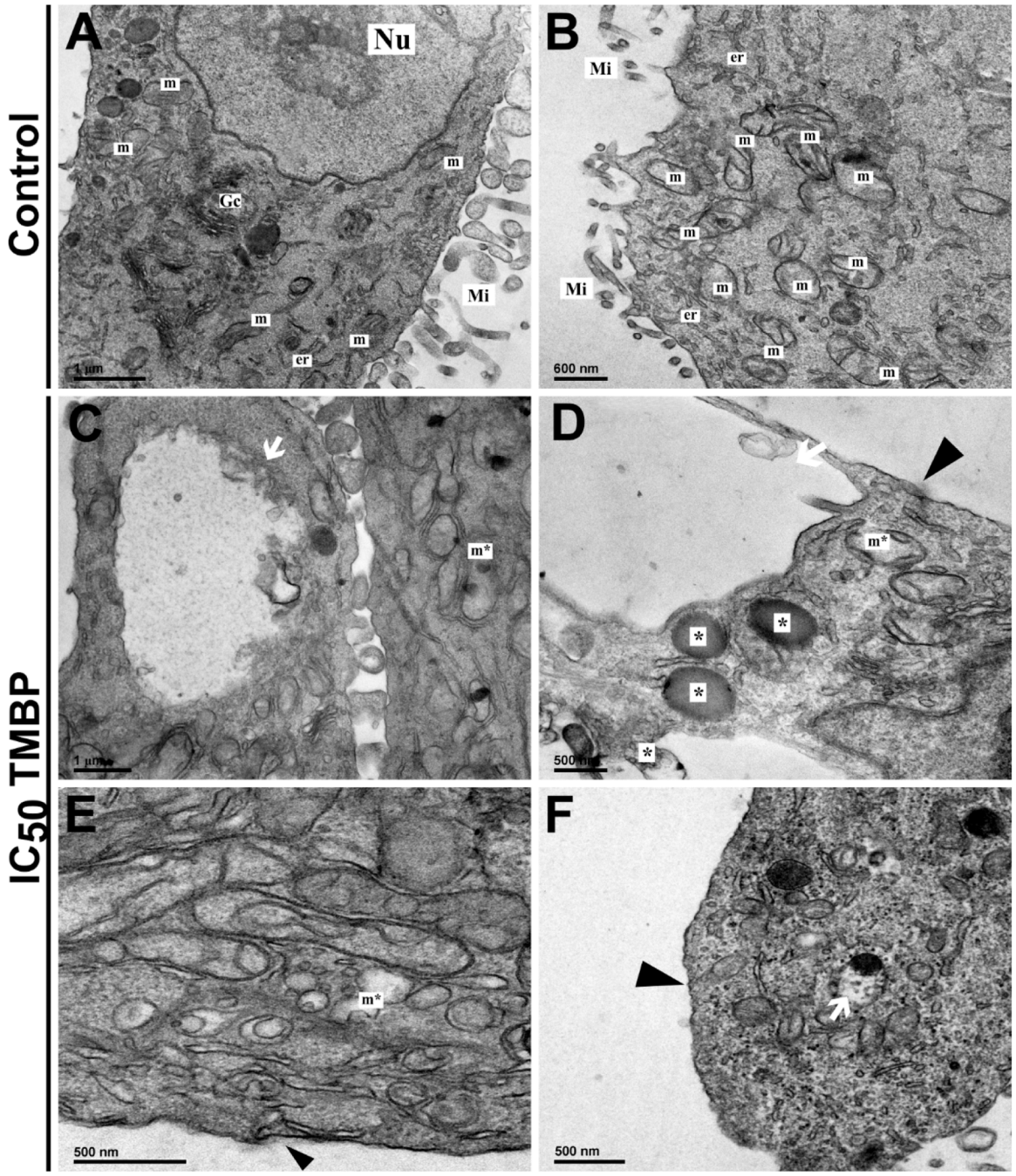

Fig. 6. : Ultrastructural changes in NCI-H460 cells treated with TMBP for 24 h and analyzed by transmission electron microscopy. (A-B) untreated cells; (C-F) cells treated with IC_{50} TMBP (152 μM); (m) mitochondria; (Gc) Golgi complex; (er) endoplasmic reticulum; (m*) mitochondrial swelling; (Nu) nucleus; (white arrow) cytoplasmic autophagic vacuole (black arrowhead) absence of microvilli; (*) lipid droplets storage areas. Scale bars = 1 μm (A, C), 600 nm (B) and 500 nm (D-F).

in N-cadherin is in line with our hypothesis that TMBP counteracts the EMT process. N-cadherin is typically upregulated during EMT and contributes to cell migration and invasion [44,48–50]. Therefore, the reduction in N-cadherin levels supports the potential anti-metastatic activity of TMBP [51–53]. In addition to its effects on metastasis-related markers, our experimental data demonstrates that TMBP not only reduces cell proliferation but also diminishes the cells' migratory capacity. Moreover, we observed that TMBP decreases cell protrusion extensions, including lamellipodia and filopodia, as well as microvilli. These observations suggest that TMBP interferes with cell locomotion by altering their invasive morphology, leading to reduced actin filament content, which subsequently impacts their motility and cell-cell adhesion.

Oxidative stress is defined as an excess of oxidants over antioxidant activity and leads to many diseases. Understanding the role of oxidative stress in cancer pathophysiology is necessary since these biomolecules impact the whole organism. Regulation of the redox state in a normal environment is critical for cellular maintenance, including viability, proliferation, and metabolism. Cells generate ROS and reactive nitrogen species (RNS), as an unavoidable consequence of physiological processes and for intracellular signaling. The major components comprising ROS are $O_2\bullet^-$, hydroxyl radical ($OH\bullet$), and hydrogen peroxide (H_2O_2). The main site of $O_2\bullet^-$ production is the mitochondria, which are used for energy production and result from the process of OXPHOS. Superoxide anion radical can be dismutated spontaneously to H_2O_2 or by the action of SODs, mainly SOD2. H_2O_2 can be catalytically converted to H_2O and

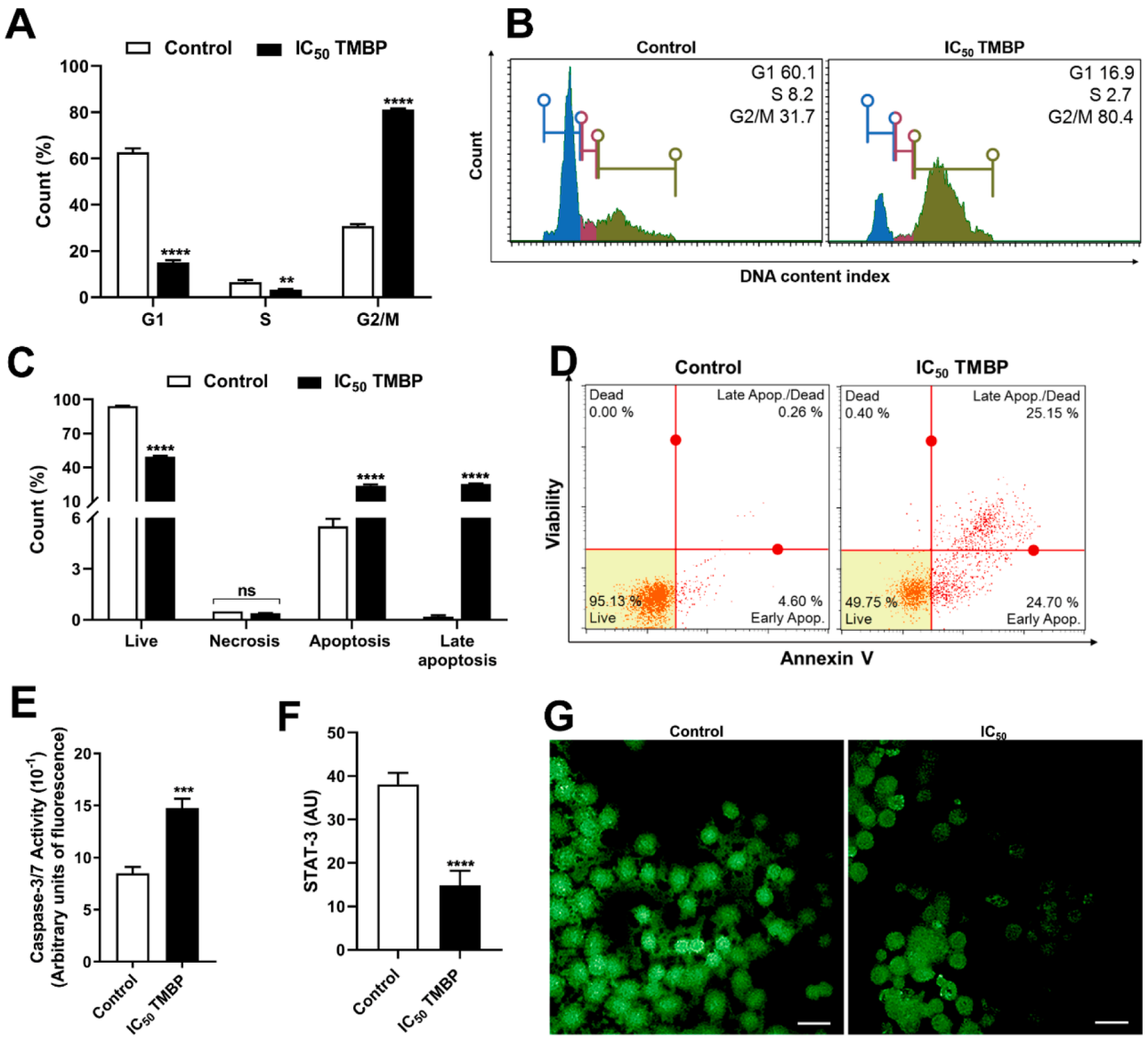

Fig. 7. : TMBP treatment induced cell cycle arrest in the G2/M phase, apoptosis, and reduced STAT-3 immunofluorescence staining in NCI-H460 cells. Cells were treated with IC_{50} of TMBP for 24 h and cell cycle distribution and histogram were quantified (A) and analyzed (B), respectively by flow cytometry. Quantitative analysis of viable, apoptotic, and necrotic NCI-H460 cells was evaluated in 24 h (C). For analysis in dot plots of cytometry, the induction of viable cells, apoptosis, and necrosis were evaluated for 24 h (D). Caspase 3/7 was quantified by fluorescence (E). Immunofluorescence staining of TMBP-treated and control cells to show reduced STAT-3 presence (green) after 24 h (F-G). Values are expressed as mean ± SEM. Cytometry data are expressed as percentage vs. control; and mean ± standard deviation. $p \leq 0.01$; * **p ≤ 0.001; * ** * $p \leq 0.0001$ vs. control. Scale bars = 20 μm (G).

O_2 by catalase, peroxiredoxins (PRDXs), and glutathione peroxidases (GPXs). GPXs require glutathione (GSH); reducing the levels of H_2O_2. Superoxide radical anion can also react with H_2O_2 to form OH•, a highly reactive radical that can damage proteins, lipids, carbohydrates, and DNA [54–56]. It should also be noted that when SOD2 activity is increased, proliferating cells go into quiescence, i.e. they do not multiply, but remain metabolically active, resulting in increased H_2O_2 activity [57].

Nitric oxide (NO) and peroxynitrite anion ($ONOO^-$) are the major RNS. GSH is highly abundant in all cellular compartments and is the main soluble antioxidant and determinant of oxidative stress. GSH also contributes to the scavenging of NO, the reduction of $ONOO^-$ and the denitrosylation of proteins. Thus, $O_2•^-$ and $ONOO^-$ are highly reactive species that can damage intracellular macromolecules, including poly-unsaturated fatty acids and nucleic acids [58,59]. Therefore, in our study, TMBP was able to reduce cancer cell viability via a ROS- and NO-dependent mechanism. Furthermore, TMBP treatment caused a reduction in $O_2•^-$ levels, increased SOD2 activity, and decreased GSH, suggesting that the highly unstable superoxide radical anions may be converted to peroxynitrite and/or hydroxyl radical.

Cancer cells exhibit aberrant metabolism, which is used to maintain their vital functions. This leads to the activation of pro-tumorigenic signaling, increased cell proliferation, migration, invasion, inhibition of apoptosis, therapeutic resistance, progression, and other aggressive features. Therefore, when cancer cells are presented with a high demand for oxidative stress, they initiate the process of adaptation in order to mitigate the damage and escape death [60,61]. Another prominent feature is the Warburg effect, which refers to the metabolic shift in cancer cells from OXPHOS to aerobic glycolysis. This glycolytic shift leads to a dramatic increase in glucose uptake and consequent lactate production, which are essential in providing substrates for cancer cells to sustain a high rate of proliferation [62–64]. Furthermore, glucose

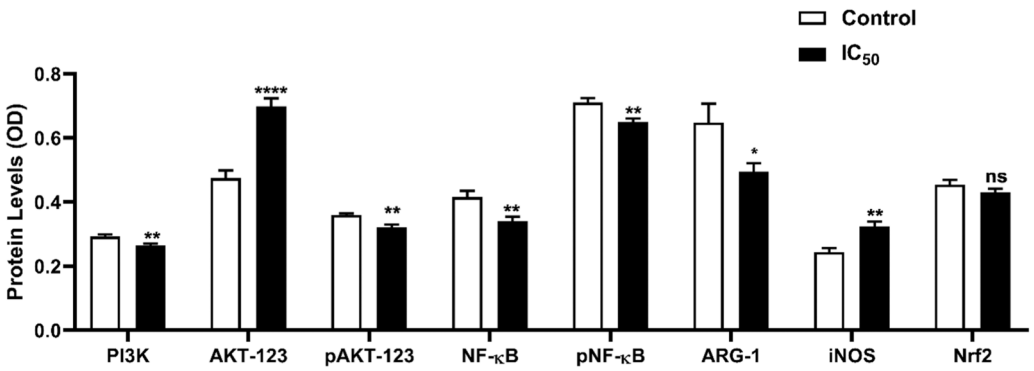

Fig. 8. : Evaluation of intracellular signaling mediators involved in the pathogenesis of lung cancer cells. ELISA measurement of PI3K, AKT, pAKT, ARG-1, iNOS, NF-κB, pNF-κB and Nrf2 levels, expressed as the natural logarithm of absorbance. White bars represent untreated NCI-H460 cells, while black bars represent 24-h TMBP-treated cells. Values represent the mean ± SEM. * ($p < 0.05$); * * ($p \leq 0.01$); * ** * ($p \leq 0.0001$); ns (not significant).

metabolism is a hallmark of NSCLC [65,66].

In addition to glycolysis, mitochondrial function, lipid biogenesis, and autophagy, although essential in physiological processes, also play a critical role in cancer development by providing cells with considerable flexibility, such as changes in utilization and energy supply, and oxidative stress management. It has also been reported that when these processes become irreparably damaged, the cell tends to undergo apoptosis [67–74]; [29–33]. In our study, we observed that TMBP treatment of NCI-H460 cells was capable of reducing glucose and lactate consumption, indicating that the cancer cells were under metabolic stress. We also found that TMBP altered mitochondrial function, as demonstrated by [19], suggesting that the cells were damaged, as confirmed by the intra- and extra-cellular LDH levels. Additionally, TMBP treatment increased lipid droplets and autophagic vacuoles; indicative of a metabolic stress profile, as confirmed by the TEM images. Taken together, these data suggest that TMBP-treated NCI-H460 cells were damaged and initiated a process of metabolic stress in an attempt for the cells to regain viability.

Controlling or terminating the uncontrolled growth of cancer cells using their own death mechanism is a highly effective method of treating cancer. Apoptosis is an essential event in the regulation of a wide range of physiological cellular processes. However, dysfunction of the apoptotic machinery is implicated in many diseases, particularly cancer. Failure to activate the apoptotic pathway can lead to chemotherapeutic resistance, tumor recurrence, and cell migration [75,76]. DNA damage, cellular and metabolic stress are known triggers of cell death by apoptosis or senescence that can eliminate dysfunctional and dangerous conditions in cells. According to our data, TMBP was able to induce cell cycle arrest, culminating in apoptosis with activation of caspase-3 and − 7. The functions of these proteases in apoptosis overlap, although they have different functions [77], with caspase-3 controlling DNA fragmentation and morphological changes, while caspase-7 is associated with loss of cell viability [78,79]. TMBP treatment was also able to reduce STAT-3 protein immunolabeling, which favors reduced migration, invasion, and metastasis.

Another important transcription factor involved with the evolution of neoplastic cells is NF-κB, which manifests a response against invading pathogens, and also promotes a metabolic switch to glycolysis and controls the tumor microenvironment in several types of cancer [80]. Furthermore, NF-κB communicates with PI3K/AKT signaling to promote the survival and proliferation of lung cancer cells [81]. The PI3K/AKT/mTOR pathway represents an attractive target for novel anticancer therapies in NSCLC, as it is also involved in the regulation of cell growth, metabolism, and resistance to therapeutic agents [34]. Judging from our data, TMBP was able to act on this pathway by reducing the levels of PI3K/AKT/NF-κB.

Another molecule of interest in cancer is the enzyme ARG-1, which has been implicated in cancer progression through several signaling pathways. ARG-1, when positively regulated, increases the levels of phosphorylated AKT and ERK, leading to cancer cell viability and proliferation. In addition, phosphorylated STAT-3 binds directly to the promoter region of ARG-1, promoting a more aggressive cancer condition. Moreover, there is evidence that patients with NSCLC have high plasma levels of ARG-1, which may be a promising target for clinical use. ARG-1 may also regulate cellular NO production by competing with iNOS for the substrate L-arginine. When produced by M2-type macrophages, ARG-1 can modulate NO production and promote tissue repair and remodeling, production of collagen and other components of the extracellular matrix. However, when iNOS metabolizes arginine to L-citrulline and NO, the latter at high concentrations (μM range) induce cellular cytotoxicity, DNA damage, nitrosation/oxidative stress, and apoptosis [82]. Thus, TMBP treatment was able to decrease ARG-1 levels and increase iNOS in NCI-H460 cells.

The effective response of TMBP against the NCI-H460 tumor cell line was due to the reduction in cell proliferation, invasive and metastatic activity, and induced morphological and ultrastructural changes in the lung cancer cells by increasing toxic mediators as oxidative species and metabolic stress, leading to a resolution of the tumor environment.

5. Conclusion

The development of therapies is a recent research trend as these are capable of reducing side effects and can improve efficacy. The use of the biotransformed compound TMBP in lung cancer has not been reported, and our study is the first to evaluate the effect of TMBP treatment on the viability of lung cancer cells and its biological mechanism and focused on the development of cell growth and apoptosis. TMBP was capable of reducing proliferation, migration, and invasion, as well as morphological and ultrastructural changes in NCI-H460 cells. TMBP treatment increased oxidative stress parameters and induced metabolic changes culminating in apoptotic death. TMBP negatively regulated proliferation-related proteins such as PI3K/AKT/NF-κB/ARG-1 and positively regulated the pro-oxidant profile mediated by the iNOS pathway.

Considering that non-small cell lung cancer (NSCLC) encompasses diverse histological subtypes, including large cell carcinoma, squamous cell carcinoma, adenocarcinoma, and adenosquamous carcinoma, our study focuses primarily on the NCI-H460 large cell carcinoma cell line and the A549 adenocarcinoma cell line, as indicated by previous research (Concato et al., 2020). These results suggest the potential broad-spectrum efficacy of TMBP against various lung cancer cells. However, it is essential to emphasize that additional investigations in different NSCLC cell lines are imperative to confirm these findings.

In light of these promising outcomes, compounds with the ability to induce cancer cell death are potential candidates for oncotherapy. Future studies should deeper into exploring the potential tumor-

suppressing effects of TMBP, thereby advancing our understanding and potentially contributing to the development of novel therapeutic approaches for lung cancer.

Funding

Not applicable.

CRediT authorship contribution statement

Virginia Marcia Concato: Conceptualization; Data curation; Formal analysis; Investigation; Methodology; Roles/Writing - original draft. **Taylon Felipe Silva:** Conceptualization; Formal analysis; Investigation; Resources; Methodology; Roles/Writing - original draft. **Mariana Barbosa Detoni:** Conceptualization; Data curation; Formal analysis; Investigation; Methodology; Roles/Writing - original draft. **Ellen Mayara Souza Cruz:** Data curation; Formal analysis; Investigation; Methodology. **Manoela Daiele Gonçalves:** Data curation; Formal analysis; Investigation; Resources; Methodology. **Bruna Taciane da Silva Bortoleti:** Data curation; Formal analysis; Investigation; Resources; Methodology. **Fernanda Tomiotto-Pellissier:** Formal analysis; Investigation; Resources; Methodology. **Ana Carolina Jacob Rodrigues:** Formal analysis; Investigation; Resources; Methodology. **Amanda Cristina Carloto:** Formal analysis; Investigation; Resources; Methodology. **Jéseka Gabriela Schirmann:** Formal analysis; Investigation; Resources; Methodology. **Aneli M. Barbosa-Dekker**: Formal analysis; Investigation; Resources; Methodology. **Robert F. H. Dekker:** Data curation; Formal analysis; Investigation; Resources; Methodology; Roles/Writing - original draft. **Ivete Conchon-Costa:** Funding acquisition; Writing - review & editing; Resources. **Carolina Panis:** Methodology; Writing - review & editing. **Danielle Bidóia Lazarin:** Methodology; Writing - review & editing. **Milena Menegazzo Miranda-Sapla:** Writing - review & editing; Data curation; Formal analysis. **Mario Sergio Mantovani:** Data curation; Formal analysis; Investigation; Resources; Methodology; Roles/Writing - original draft. **Wander Rogério Pavanelli:** Funding acquisition; Project administration; Supervision; Validation; Writing - review & editing; Resources.

Declaration of Competing Interest

The authors declare that they have no competing interests.

Data availability

Data will be made available on request.

Acknowledgments

This work was supported by the Coordenaç ão de Aperfeiçoamento de Pessoal de N í vel Superior (CAPES, Brazil), Conselho Nacional de Pesquisa (CNPq, Brazil), Financiadora de Estudos e Projetos (FINEP) and Universidade Estadual de Londrina (UEL, Brazil).

Appendix A. Supporting information

Supplementary data associated with this article can be found in the online version at doi:10.1016/j.biopha.2023.115979.

References

[1] F. Bray, J. Ferlay, I. Soerjomataram, R.L. Siegel, L.A. Torre, A. Jemal, Global cancer statistics 2018: GLOBOCAN estimates of incidence and mortality worldwide for 36 cancers in 185 countries, CA Cancer J. Clin. 68 (2018) 394–424, https://doi.org/10.3322/caac.21492.

[2] M.B. Schabath, M.L. Cote, Cancer progress and priorities: lung cancer, Cancer Epidemiol. Biomark. Prev. 28 (2019) 1563–1579, https://doi.org/10.1158/1055-9965.EPI-19-0221.

[3] V.S. Iglesias, L. Giuranno, L.J. Dubois, J. Theys, M. Vooijs, Drug resistance in non-small cell lung cancer: a potential for NOTCH targeting? Front. Oncol. 8 (2018) 267, https://doi.org/10.3389/FONC.2018.00267.

[4] S. Dasari, P. Bernard Tchounwou, Cisplatin in cancer therapy: molecular mechanisms of action, Eur. J. Pharmcol. 740 (2014) 364–378, https://doi.org/10.1016/J.EJPHAR.2014.07.025.

[5] F. Von Nussbaum, M. Brands, B. Hinzen, S. Weigand, D. Häbich, Antibacterial natural products in medicinal chemistry–exodus or revival? Angew. Chem. Int. Ed. Engl. 45 (2006) 5072–5129, https://doi.org/10.1002/ANIE.200600350.

[6] Z. Rasines-Perea, R. Jacquet, M. Jourdes, S. Quideau, P.L. Teissedre, Ellagitannins and flavano-ellagitannins: red wines tendency in different areas, barrel origin and ageing time in barrel and bottle, Biomolecules 9 (2019), https://doi.org/10.3390/BIOM9080316.

[7] J.G. Schirmann, R.F.H. Dekker, D. Borsato, A.M. Barbosa-Dekker, Selective control for the laccase-catalyzed synthesis of dimers from 2,6-dimethoxyphenol: optimization of 3,3',5,5'-tetramethoxy-biphenyl-4,4'-diol synthesis using factorial design, and evaluation of its antioxidant action in biodiesel, Appl. Catal. A Gen. 555 (2018) 88–97, https://doi.org/10.1016/J.APCATA.2018.02.015.

[8] J.G. Schirmann, K.G. Angilelli, R.F.H. Dekker, D. Borsato, A.M. Barbosa-Dekker, 3,3″,5,5″-Tetramethoxybiphenyl-4,4″-diol: a new antioxidant enhancing oxidative stability of soybean biodiesel, Fuel 237 (2019) 593–596, https://doi.org/10.1016/J.FUEL.2018.10.044.

[9] M.D. Gonçalves, F. Tomiotto-Pellissier, R.L.N. de Matos, J.P. Assolini, B.T. da Silva Bortoleti, V.M. Concato, et al., Recent advances in biotransformation by cunninghamella species, Curr. Drug Metab. 22 (2021) 1035–1064, https://doi.org/10.2174/1389200222666211126100023.

[10] A. Kobayashi, Y. Koguchi, H. Kanzaki, I. Kajiyama, K. Kawazu, Production of a new type of bioactive phenolic compound, Biosci. Biotechnol. Biochem. 58 (1994) 133–134, https://doi.org/10.1271/BBB.58.133.

[11] K.H. Bang, Y.K. Kim, B.S. Min, M.K. Na, Y.H. Rhee, J.P. Lee, et al., Antifungal activity of Magnolol and Honokiol, Arch. Pharm. Res. 23 (2000) 46–49, https://doi.org/10.1007/BF02976465/METRICS.

[12] C. Hawkshaw, O. Kiamanesh, R. Walton, The effects of the antimicrobial honokiol on the intracellular pH of bacillus subtilis WB746 and Escherichia coli B23, J. Exp. Microbiol. Immunol. 12 (2008) 14–20.

[13] A. Kobayashi, Y. Koguchi, H. Kanzaki, I. Kajiyama, K. Kawazu, Production of a new type of bioactive phenolic compound, Biosci. Biotechnol. Biochem. 58 (1994) 133–134, https://doi.org/10.1271/BBB.58.133.

[14] R. Uta, C. François, H. Marvin, A. Philipp, P.P. Andrea, W. Henrik, et al., Anti-inflammatory properties of Honokiol in activated primary microglia and astrocytes, J. Neuroimmunol. 323 (2018) 78–86, https://doi.org/10.1016/J.JNEUROIM.2018.07.013.

[15] Y. Murakami, H. Ishii, S. Hoshina, N. Takada, A. Ueki, S. Tanaka, et al., Antioxidant and cyclooxygenase-2-inhibiting activity of 4,4′-Biphenol, 2,2′-Biphenol and Phenol, Anticancer Res. 29 (2009).

[16] C. Ramachandran, B. Wilk, S.J. Melnick, I. Eliaz, Synergistic antioxidant and anti-inflammatory effects between modified citrus pectin and honokiol, Evid. Based Complement Altern. Med. 2017 (2017), https://doi.org/10.1155/2017/8379843.

[17] C.-H. Hsiao, C.-J. Yao, G.-M. Lai, L.-M. Lee, J. Whang-Peng, P.-H. Shih, Honokiol induces apoptotic cell death by oxidative burst and mitochondrial hyperpolarization of bladder cancer cells, Exp. Ther. Med. 17 (2019) 4213, https://doi.org/10.3892/ETM.2019.7419.

[18] K. Huang, Y. Chen, R. Zhang, Y. Wu, Y. Ma, X. Fang, et al., Honokiol induces apoptosis and autophagy via the ROS/ERK1/2 signaling pathway in human osteosarcoma cells in vitro and in vivo, Cell Death Dis. 9 (2018) 1–17, https://doi.org/10.1038/s41419-017-0166-5.

[19] V.M. Concato, F. Tomiotto-Pellissier, T.F. Silva, M.D. Gonçalves, B.T. da S. Bortoleti, M.B. Detoni, et al., 3,3',5,5'-tetramethoxybiphenyl-4,4'diol induces cell cycle arrest in G2/M phase and apoptosis in human non-small cell lung cancer A549 cells, Chem. Biol. Interact. 326 (2020), https://doi.org/10.1016/J.CBI.2020.109133.

[20] J.G. Schirmann, R.F.H. Dekker, D. Borsato, A.M. Barbosa-Dekker, Selective control for the laccase-catalyzed synthesis of dimers from 2,6-dimethoxyphenol: Optimization of 3,3',5,5'-tetramethoxy-biphenyl-4,4'-diol synthesis using factorial design, and evaluation of its antioxidant action in biodiesel, Appl. Catal. A Gen. 555 (2018) 88–97, https://doi.org/10.1016/J.APCATA.2018.02.015.

[21] F. Tomiotto-Pellissier, D.R. Alves, M.M. Miranda-Sapla, S.M. de Morais, J. P. Assolini, B.T. da Silva Bortoleti, et al., Caryocar coriaceum extracts exert leishmanicidal effect acting in promastigote forms by apoptosis-like mechanism and intracellular amastigotes by Nrf2/HO-1/ferritin dependent response and iron depletion: leishmanicidal effect of Caryocar coriaceum leaf exracts, Biomed. Pharmacother. 98 (2018) 662–672, https://doi.org/10.1016/J.BIOPHA.2017.12.083.

[22] R. Duplancic, D. Kero, Novel approach for quantification of multiple immunofluorescent signals using histograms and 2D plot profiling of whole-section panoramic images, Sci. Rep. 11 (2021) 1–17, https://doi.org/10.1038/s41598-021-88101-1.

[23] A.H.D. Cataneo, F. Tomiotto-Pellissier, M.M. Miranda-Sapla, J.P. Assolini, C. Panis, D. Kian, et al., Quercetin promotes antipromastigote effect by increasing the ROS production and anti-amastigote by upregulating Nrf2/HO-1 expression, affecting iron availability, Biomed. Pharmacother. 113 (2019), 108745, https://doi.org/10.1016/J.BIOPHA.2019.108745.

[24] S. Marklund, G. Marklund, Involvement of the superoxide anion radical in the autoxidation of pyrogallol and a convenient assay for superoxide dismutase, Eur. J. Biochem. 47 (1974) 469–474, https://doi.org/10.1111/J.1432-1033.1974.TB03714.X.

[25] O.H. Lowry, N.J. Rosebrough, A.L. Farr, R.J. Randall, Protein measurement with the folin phenol reagent, J. Biol. Chem. 193 (1951) 265–275, https://doi.org/10.1016/S0021-9258(19)52451-6.

[26] I. Rahman, A. Kode, S.K. Biswas, Assay for quantitative determination of glutathione and glutathione disulfide levels using enzymatic recycling method, Nat. Protoc. 1 (2007) 3159–3165, https://doi.org/10.1038/nprot.2006.378.

[27] F.H. Khan, E. Dervan, D.D. Bhattacharyya, J.D. McAuliffe, K.M. Miranda, S. A. Glynn, The role of nitric oxide in cancer: master regulator or NOt? Int. J. Mol. Sci. 21 (2020) 1–30, https://doi.org/10.3390/IJMS21249393.

[28] B. Griess, E. Tom, F. Domann, M. Teoh-Fitzgerald, Extracellular superoxide dismutase and its role in cancer, Free Radic. Biol. Med. 112 (2017) 464, https://doi.org/10.1016/J.FREERADBIOMED.2017.08.013.

[29] C.W. Yun, S.H. Lee, The roles of autophagy in cancer, Int. J. Mol. Sci. 19 (2018), https://doi.org/10.3390/IJMS19113466.

[30] D. Grasso, L.X. Zampieri, T. Capelôa, J.A. Van De Velde, P. Sonveaux, Mitochondria in cancer, Cell Stress 4 (2020) 114, https://doi.org/10.15698/CST2020.06.221.

[31] A.L.S. Cruz, E. de A. Barreto, N.P.B. Fazolini, J.P.B. Viola, P.T. Bozza, Lipid droplets: platforms with multiple functions in cancer hallmarks, Cell Death Dis. 11 (2020) 1–16, https://doi.org/10.1038/s41419-020-2297-3.

[32] C. Wang, R.J. Youle, The role of mitochondria in apoptosis, Annu. Rev. Genet. 43 (2009) 95, https://doi.org/10.1146/ANNUREV-GENET-102108-134850.

[33] J. Boren, K.M. Brindle, Apoptosis-induced mitochondrial dysfunction causes cytoplasmic lipid droplet formation, Cell Death Differ. 19 (2012) 1561, https://doi.org/10.1038/CDD.2012.34.

[34] A.C. Tan, Targeting the PI3K/Akt/mTOR pathway in non-small cell lung cancer (NSCLC), Thorac. Cancer 11 (2020) 511, https://doi.org/10.1111/1759-7714.13328.

[35] V.S. Iglesias, L. Giuranno, L.J. Dubois, J. Theys, M. Vooijs, Drug resistance in non-small cell lung cancer: a potential for NOTCH targeting? Front. Oncol. 8 (2018) 267, https://doi.org/10.3389/FONC.2018.00267.

[36] M. Ashrafizadeh, A. Zarrabi, K. Hushmandi, F. Hashemi, E.R. Moghadam, M. Owrang, et al., Lung cancer cells and their sensitivity/resistance to cisplatin chemotherapy: role of microRNAs and upstream mediators, Cell Signal 78 (2021), 109871, https://doi.org/10.1016/J.CELLSIG.2020.109871.

[37] S. Ghosh, Cisplatin: the first metal based anticancer drug, Bioorg. Chem. 88 (2019), 102925, https://doi.org/10.1016/J.BIOORG.2019.102925.

[38] F. Gao, J.M. Zhang, Z.G. Wang, W. Peng, H.L. Hu, C.M. Fu, Biotransformation, a promising technology for anti-cancer drug development, Asian Pac. J. Cancer Prev. 14 (2013) 5599–5608, https://doi.org/10.7314/APJCP.2013.14.10.5599.

[39] M.D. Gonçalves, F. Tomiotto-Pellissier, R.L.N. de Matos, J.P. Assolini, B.T. da Silva Bortoleti, V.M. Concato, et al., Recent advances in biotransformation by Cunninghamella species, Curr. Drug Metab. 22 (2021) 1035–1064, https://doi.org/10.2174/1389200222666211126100023.

[40] D.A. Lauffenburger, A.F. Horwitz, Cell migration: a physically integrated molecular process, Cell 84 (1996) 359–369, https://doi.org/10.1016/S0092-8674(00)81280-5.

[41] M. Janiszewska, M.C. Primi, T. Izard, Cell adhesion in cancer: beyond the migration of single cells, J. Biol. Chem. 295 (2020) 2495–2505, https://doi.org/10.1074/JBC.REV119.007759.

[42] M. Bush, B.M. Alhanshali, S. Qian, C.B. Stanley, W.T. Heller, T. Matsui, et al., An ensemble of flexible conformations underlies mechanotransduction by the cadherin–catenin adhesion complex, Proc. Natl. Acad. Sci. USA 116 (2019) 21545–21555, https://doi.org/10.1073/PNAS.1911489116/SUPPL_FILE/PNAS.1911489116.SAPP.PDF.

[43] F. Péglion, S. Etienne-Manneville, N-cadherin expression level as a critical indicator of invasion in non-epithelial tumors, Cell Adhes. Migr. 6 (2012) 327, https://doi.org/10.4161/CAM.20855.

[44] C.Y. Loh, J.Y. Chai, T.F. Tang, W.F. Wong, G. Sethi, M.K. Shanmugam, et al., The E-cadherin and N-cadherin switch in epithelial-to-mesenchymal transition: signaling, therapeutic implications, and challenges, Cells 8 (2019), https://doi.org/10.3390/CELLS8101118.

[45] T. Valenta, G. Hausmann, K. Basler, The many faces and functions of β-catenin, EMBO J. 31 (2012) 2714–2736, https://doi.org/10.1038/EMBOJ.2012.150.

[46] J. Jin, P. Zhan, M. Katoh, S.S. Kobayashi, K. Phan, H. Qian, et al., Prognostic significance of β-catenin expression in patients with non-small cell lung cancer: a meta-analysis, Transl. Lung Cancer Res. 6 (2017) 97–108, https://doi.org/10.21037/TLCR.2017.02.07.

[47] W. Zhu, H. Wang, D. Zhu, Wnt/β-catenin signaling pathway in lung cancer, Med. Drug Discov. 13 (2022), 100113, https://doi.org/10.1016/J.MEDIDD.2021.100113.

[48] Y. Kang, J. Massagué, Epithelial-mesenchymal transitions: twist in development and metastasis, Cell 118 (2004) 277–279, https://doi.org/10.1016/j.cell.2004.07.011.

[49] P.V. Angadi, P.V. Patil, V. Angadi, D. Mane, S. Shekar, S. Hallikerimath, et al., Immunoexpression of epithelial mesenchymal transition proteins E-cadherin, β-catenin, and N-cadherin in oral squamous cell carcinoma, Int. J. Surg. Pathol. 24 (2016) 696–703, https://doi.org/10.1177/1066896916654763.

[50] Y. Miao, A.L. Li, L. Wang, C.F. Fan, X.P. Zhang, H.T. Xu, et al., Overexpression of NEDD9 is associated with altered expression of E-Cadherin, β-Catenin and N-Cadherin and predictive of poor prognosis in non-small cell lung cancer, Pathol. Oncol. Res. 19 (2013) 281–286, https://doi.org/10.1007/S12253-012-9580-2.

[51] H. Sun, M. Liu, X. Wu, C. Yang, Y. Zhang, Z. Xu, et al., Overexpression of N-cadherin and β-catenin correlates with poor prognosis in patients with nasopharyngeal carcinoma, Oncol. Lett. 13 (2017) 1725, https://doi.org/10.3892/OL.2017.5645.

[52] J. shun Wu, J. Jiang, B. jun Chen, K. Wang, Y. ling Tang, X. hua Liang, Plasticity of cancer cell invasion: patterns and mechanisms, Transl. Oncol. 14 (2021), 100899, https://doi.org/10.1016/J.TRANON.2020.100899.

[53] K.M. Mrozik, O.W. Blaschuk, C.M. Cheong, A.C.W. Zannettino, K. Vandyke, N-cadherin in cancer metastasis, its emerging role in haematological malignancies and potential as a therapeutic target in cancer, BMC Cancer 18 (2018) 1–16, https://doi.org/10.1186/S12885-018-4845-0.

[54] E. Birben, U.M. Sahiner, C. Sackesen, S. Erzurum, O. Kalayci, Oxidative stress and antioxidant defense, World Allergy Organ J. 5 (2012) 9, https://doi.org/10.1097/WOX.0B013E3182439613.

[55] J.D. Hayes, A.T. Dinkova-Kostova, K.D. Tew, Oxidative stress in cancer, Cancer Cell 38 (2020) 167, https://doi.org/10.1016/J.CCELL.2020.06.001.

[56] M. Azmanova, A. Pitto-Barry, Oxidative stress in cancer therapy: friend or enemy? ChemBioChem 23 (2022), e202100641 https://doi.org/10.1002/CBIC.202100641.

[57] M. Wang, J.S. Kirk, S. Venkataraman, F.E. Domann, H.J. Zhang, F.Q. Schafer, et al., Manganese superoxide dismutase suppresses hypoxic induction of hypoxia-inducible factor-1alpha and vascular endothelial growth factor, Oncogene 24 (2005) 8154–8166, https://doi.org/10.1038/SJ.ONC.1208986.

[58] M.V. Beligni, L. Lamattina, Is nitric oxide toxic or protective? Trends Plant Sci. 4 (1999) 299–300, https://doi.org/10.1016/s1360-1385(99)01451-x.

[59] R. Radi, Oxygen radicals, nitric oxide, and peroxynitrite: redox pathways in molecular medicine, Proc. Natl. Acad. Sci. USA 115 (2018) 5839–5848, https://doi.org/10.1073/PNAS.1804932115/ASSET/52782DFA-96E3-4150-AB66-C339B5F09458/ASSETS/GRAPHIC/PNAS.1804932115FIG03.JPEG.

[60] S. Arfin, N.K. Jha, S.K. Jha, K.K. Kesari, J. Ruokolainen, S. Roychoudhury, et al., Oxidative stress in cancer cell metabolism, Antioxidants Vol 10 (2021) 642, https://doi.org/10.3390/ANTIOX10050642.

[61] F. Xing, Q. Hu, Y. Qin, J. Xu, B. Zhang, X. Yu, et al., The relationship of redox with hallmarks of cancer: the importance of homeostasis and context, Front Oncol. 12 (2022) 1437, https://doi.org/10.3389/FONC.2022.862743/BIBTEX.

[62] K.M. Yap, M. Sekar, Y.S. Wu, S.H. Gan, N.N.I.M. Rani, L.J. Seow, et al., Hesperidin and its aglycone hesperetin in breast cancer therapy: a review of recent developments and future prospects, Saudi J. Biol. Sci. 28 (2021) 6730–6747, https://doi.org/10.1016/J.SJBS.2021.07.046.

[63] P. Wee, Z. Wang, Epidermal growth factor receptor cell proliferation signaling pathways, Cancers (Basel) 9 (2017), https://doi.org/10.3390/CANCERS9050052.

[64] S. Cassim, M. Vučetić, M. Ždralević, J. Pouyssegur, Warburg and beyond: the power of mitochondrial metabolism to collaborate or replace fermentative glycolysis in cancer, Cancers 12 (2020), https://doi.org/10.3390/CANCERS12051119.

[65] J. Boren, K.M. Brindle, Apoptosis-induced mitochondrial dysfunction causes cytoplasmic lipid droplet formation, Cell Death Differ. 19 (2012) 1561, https://doi.org/10.1038/CDD.2012.34.

[66] J.Q. Xu, Y.L. Fu, J. Zhang, K.Y. Zhang, J. Ma, J.Y. Tang, et al., Targeting glycolysis in non-small cell lung cancer: promises and challenges, Front Pharmacol. 13 (2022), https://doi.org/10.3389/FPHAR.2022.1037341.

[67] S. Cassim, M. Vučetić, M. Ždralević, J. Pouyssegur, Warburg and beyond: the power of mitochondrial metabolism to collaborate or replace fermentative glycolysis in cancer, Cancers 12 (2020), https://doi.org/10.3390/CANCERS12051119.

[68] E. White, Role of metabolic stress responses of apoptosis and autophagy in tumor suppression, Ernst Scher. Found. Symp. Proc. (2007) 23, https://doi.org/10.1007/2789_2008_087.

[69] W. Guo, K. Du, S. Luo, D. Hu, Recent advances of autophagy in non-small cell lung cancer: from basic mechanisms to clinical application, Front. Oncol. 12 (2022), https://doi.org/10.3389/FONC.2022.861959.

[70] C.H. Chuang, M. Dorsch, P. Dujardin, S. Silas, K. Ueffing, J.M. Holken, et al., Altered mitochondria functionality defines a metastatic cell state in lung cancer and creates an exploitable vulnerability, Cancer Res. 81 (2021) 567, https://doi.org/10.1158/0008-5472.CAN-20-1865.

[71] W. Luo, H. Wang, L. Ren, Z. Lu, Q. Zheng, L. Ding, et al., Adding fuel to the fire: The lipid droplet and its associated proteins in cancer progression, Int. J. Biol. Sci. 18 (2022) 6020–6034, https://doi.org/10.7150/IJBS.74902.

[72] D. Grasso, L.X. Zampieri, T. Capelôa, J.A. Van De Velde, P. Sonveaux, Mitochondria in cancer, Cell Stress 4 (2020) 114, https://doi.org/10.15698/CST2020.06.221.

[73] T. Petan, E. Jarc, M. Jusović, Lipid droplets in cancer: guardians of fat in a stressful world, Molecules Vol 23 (2018) 1941, https://doi.org/10.3390/MOLECULES23081941.

[74] C.W. Yun, S.H. Lee, The roles of autophagy in cancer, Int. J. Mol. Sci. 19 (2018), https://doi.org/10.3390/IJMS19113466.

[75] K. Mehdizadeh, F. Ataei, S. Hosseinkhani, Treating MCF7 breast cancer cell with proteasome inhibitor Bortezomib restores apoptotic factors and sensitizes cell to Docetaxel, Med. Oncol. 38 (2021) 1–8, https://doi.org/10.1007/S12032-021-01509-7/FIGURES/4.

[76] C.M. Pfeffer, A.T.K. Singh, Apoptosis: a target for anticancer therapy, Int. J. Mol. Sci. 19 (2018), https://doi.org/10.3390/IJMS19020448.

[77] J.G. Walsh, S.P. Cullen, C. Sheridan, A.U. Lüthi, C. Gerner, S.J. Martin, Executioner caspase-3 and caspase-7 are functionally distinct proteases, Proc. Natl. Acad. Sci. USA 105 (2008) 12815–12819, https://doi.org/10.1073/PNAS.0707715105/SUPPL_FILE/0707715105SI.PDF.

[78] M. Brentnall, L. Rodriguez-Menocal, R.L. De Guevara, E. Cepero, L.H. Boise, Caspase-9, caspase-3 and caspase-7 have distinct roles during intrinsic apoptosis, BMC Cell Biol. 14 (2013) 1–9, https://doi.org/10.1186/1471-2121-14-32/FIGURES/5.

[79] S.A. Lakhani, A. Masud, K. Kuida, G.A. Porter, C.J. Booth, W.Z. Mehal, et al., Caspases 3 and 7: key mediators of mitochondrial events of apoptosis, Science 311 (2006) 847, https://doi.org/10.1126/SCIENCE.1115035.
[80] K. Taniguchi, M. Karin, NF-κB, inflammation, immunity and cancer: coming of age, Nat. Rev. Immunol. 18 (2018) 309–324, https://doi.org/10.1038/NRI.2017.142.
[81] W. Chen, Z. Li, L. Bai, Y. Lin, NF-kappaB, a mediator for lung carcinogenesis and a target for lung cancer prevention and therapy, Front. Biosci. 16 (2011) 1172, https://doi.org/10.2741/3782.
[82] F. Niu, Y. Yu, Z. Li, Y. Ren, Z. Li, Q. Ye, et al., Arginase: An emerging and promising therapeutic target for cancer treatment, Biomed. Pharmacother. 149 (2022), 112840, https://doi.org/10.1016/J.BIOPHA.2022.112840.